JVST A
Journal of Vacuum Science & Technology A

ARTICLE

pubs.aip.org/avs/jva

Consequences of low bias frequencies in inductively coupled plasmas on ion angular distributions for high aspect ratio plasma etching

Cite as: J. Vac. Sci. Technol. A 43, 033001 (2025); doi: 10.1116/6.0004250
Submitted: 29 November 2024 · Accepted: 21 February 2025 ·
Published Online: 10 March 2025

Evan Litch,[1,a)] Hyunjae Lee,[2,a)] Sang Ki Nam,[2,a)] and Mark J. Kushner[3,a)]

AFFILIATIONS

[1]Nuclear Engineering and Radiological Sciences Department, University of Michigan, 2355 Bonisteel Blvd, Ann Arbor, Michigan 48109
[2]Mechatronics R&D Center, Samsung Electronics Co., Ltd., 1-1 Samsungjeonja-ro, Hwaseong-si, Gyeonggi-do 18448, South Korea
[3]Electrical Engineering and Computer Science Department, University of Michigan, 1301 Beal Ave., Ann Arbor, Michigan 48109-2122

[a)]**Authors to whom correspondence should be addressed:** elitch@umich.edu; hj0928.lee@samsung.com; sangki.j.nam@samsung.com; and mjkush@umich.edu

ABSTRACT

Plasma etching of high aspect ratio (HAR) features for microelectronics fabrication is becoming increasingly challenging due to the increasing aspect ratio and tighter tolerances on the required anisotropy of the angular distribution of ions onto the wafer. These HAR features include deep trench isolation which after etching are filled with dielectric material to electrically isolate devices. A strategy to increase ion energy and narrow angular distributions onto the wafer is to operate with substrate biases at low frequencies, typically below a few MHz to several hundred kHz. Maintaining desired properties of the ion energy and angular distributions (IEADs) to the edge of the wafer is also becoming more challenging, leading to edge exclusion—a portion of the wafer at its outer edge that does not yield high quality devices. Deviation of IEADs from the ideal at the edge of the wafer is usually due to a tilt from the normal. The tilt is generally associated with curvature of the sheath that accelerates ions into the wafer, transitioning from the edge of the wafer to the focus ring, a dielectric that surrounds the wafer. In this paper, we report on a computational investigation of IEADs incident on the wafer as a function of radius in an inductively coupled plasma (ICP) sustained in $Ar/Cl_2/O_2$ mixtures with substrate biases from 250 kHz to 5 MHz. Curvature of the sheath at the wafer edge leading to a tilt of the IEAD results, to first order, from charging of the focus ring that thins the sheath above the focus ring relative to that over the wafer. This charging is frequency dependent, with more charging and sheath curvature occurring at lower bias frequencies. The consequences on sheath curvature and tilt of the IEAD due to bias voltage, ICP power, and electrical properties of the focus ring are discussed. Limiting thinning of the sheath and reducing charging of the focus ring generally reduce sheath curvature and improve anisotropy of the IEADs in the edge region of the wafer.

I. INTRODUCTION

With reductions in feature size in semiconductor device memory architectures having slowed, emphasis is increasingly being placed on stacking layers of memory cells to increase memory area density.[1] A consequence of fabricating layered three-dimensional (3D) devices is the need to plasma etch high aspect ratio (HAR) features.[2–4] For example, 3D-NAND memory structures are fabricated beginning with initially hundreds of alternating layers of SiO_2 and Si_3N_4 requiring vias having aspect ratio (AR) >100 to be etched.[5] These dielectric features are generally etched with fluorocarbon gas mixtures using capacitively coupled plasmas.[5,6] Another class of HAR feature is deep trench isolation (DTI) which is used to electrically isolate 3D logic and imaging devices.[7] DTI begins as etched trenches which are coated with a dielectric such as SiO_2 and backfilled with polysilicon to produce a series capacitance between devices. Charging of the capacitance of the DTI structures then electrically isolates the devices by blocking lower frequency current. Plasma etching of DTI structures typically occurs in conductive substrates such as Si, often with overlying layers of SiO_2 and Si_3N_4, etched with halogen containing gas mixtures (e.g., HBr or Cl_2)

processed in inductively coupled plasmas (ICPs) with a capacitively coupled substrate bias.

Plasma etching of HAR DTI structures places strict requirements on the energies and angular distributions of ions incident onto the wafer. In order to reduce the sidewall etch rate (or to customize the sidewall slope) with increasing AR, ion trajectories require increasingly narrower angular distributions while having higher energies so that ions retain sufficient energy to activate etching after glancing sidewall collisions. High voltages (several kilovolts) are often applied as substrate basis to achieve these high energy and narrow angular ion trajectories.[1,8,9] Under such conditions, the etch rate typically scales in proportion to the square root of the ion energy and bias voltage.[10,11] Increasing bias voltage to increase etch rate implies a commensurate increase in bias power, which at some point has a practical limit.

One proposed remedy to reduce the need to increase bias voltage is to reduce the frequency of the biased applied to the substrate.[12] By reducing the frequency of the bias, the ion energy distribution (IED) broadens in energy to produce a bimodal structure, while extending the highest ion energies onto the wafer to nearly the maximum allowed (V_o–V_{DC}, where V_o is the amplitude of the applied bias and V_{DC} is the DC bias, which is usually negative).[13,14] Both the higher maximum energies and proportionately narrower ion angular distributions (IADs) have the potential to improve the anisotropic etch rate for HAR features. The range of radio frequency (rf) biases applied to the substrate with the intent of controlling IEADs (ion energy and angular distributions) to the wafer are hundreds of kHz to many tens of MHz. The range of frequencies below 1 MHz is often referred to as very low frequency (VLF) biases.

Maintaining the uniformity of the ion and radical fluxes to the wafer is critical to improving yield in high volume manufacturing. Maintaining uniformity is particularly challenging in the last few millimeters of the outer radius of the wafer where the quality of etching often degrades. This degradation in quality of the etch is often referred to as edge exclusion.[15] One component of edge exclusion is ion tilt, where ions incident onto the wafer arrive with an angle offset from the vertical or normal.

Ion tilt can occur at any point on the wafer where the electric field in the sheath has components that are offset from the normal. For example, the sheath may not be parallel to the wafer due to a nonuniform plasma density above the wafer. Since the wafer is itself conductive (or if nonconductive will acquire surface charge), electric fields tend to be normal to the surface of the wafer. The electric field also tends to be normal to the sheath edge. If the sheath edge is not parallel to the wafer, then the electric field will have curvature through the sheath transitioning from the wafer surface to the sheath edge. Even if the sheath is parallel to the wafer and electric fields in the sheath are normal to the wafer, ions that arrive at the sheath edge and enter the sheath with a non-normal velocity will strike the wafer with a tilt. So, tilt can originate far from the sheath edge.

Sheath curvature here refers to the transition in thickness of the sheath crossing over the edge of the wafer and which produces electric field components that are not normal to the wafer. Sheath curvature results dominantly from two processes. With sheath thickness being inversely proportional to plasma density, a gradient in plasma density at the edge of the wafer translates into a gradient in sheath thickness (or sheath curvature) which then contributes to ion tilt. These non-normal electric fields then accelerate ions across the sheath with a non-normal angle.[16–20] The precise relationship between ion tilt and sheath curvature has not been definitively experimentally established as there are other contributing factors, such as the velocity of the ion approaching the sheath.

The second is a change in the electrical properties of the substrate beyond the edge of the wafer. The sheath represents a capacitive impedance in series with the impedance of the underlying substrate. The sheath voltage to some degrees results from voltage division between the series impedance of the sheath, the bulk plasma, and the underlying substrate, with more voltage allocated to the larger impedance and smaller capacitance. Sheath thickness scales with sheath voltage. With a change in impedance of the underlying substrate, from over the wafer to beyond the edge of the wafer, the proportion of voltage allocated to the sheath changes. This change in sheath voltage in turn changes the sheath thickness. A gradient in sheath thickness (sheath curvature) then leads to a tilt in the ion angular distribution.

Plasma equipment designers have developed several remedies for edge exclusion and ion tilt at the edge of the wafer, often in the form of engineering focus rings. The focus ring (FR) is a structure surrounding the wafer having the goal of minimizing edge exclusion by making plasma produced reactant fluxes uniform across the edge of the wafer, reducing sheath curvature and minimizing ion tilt. FR engineering is not independent of the choice of frequency for the applied bias. The FR material and structures are typically dielectrics having electrical impedances that are functions of frequency. With everything else remaining constant, a change in frequency of the applied bias results in a change in impedance of the FR and so a change in voltage division between the underlying substrate (the FR) and the sheath. This change in sheath voltage produces a change in sheath width and produces sheath curvature. Changing the height of the focus ring relative to the wafer can also compensate for curvature of the sheath produced by differences in sheath thickness.[18] The consequences of transitioning to VLF for substrate bias and the resulting change in impedance of the FR on sheath thickness, sheath curvature, and ion tilt are not well understood.[21–23]

In this work, we report on results from simulations conducted for a range of substrate bias frequencies in an ICP sustained in an $Ar/Cl_2/O_2$ mixture as typically used for etching HAR features for DTI. The goal is to investigate the consequences of VLF biases on the IEADs approaching the edge of the wafer and its relation to FR properties. An ICP reactor was chosen for this investigation due to its prevalent use for DTI fabrication and the ability to separate source power for plasma generation from ion acceleration produced by the biased electrode for moderately low frequency biases. We found that ion tilt approaching the edge of the wafer depends on bias frequency and the capacitance of the FR. For otherwise constant bulk plasma properties, the dielectric constant of the FR determines the RC (resistance–capacitance) time constant for charging the capacitance of the FR. High bias frequencies having RF periods shorter than the RC time constant for charging the FR will pass current through the FR during the entire RF period, producing thicker sheaths above the FR and less sheath curvature at the edge of the wafer. VLF biases having RF periods longer than the RC

time constant for charging the FR will charge the FR, producing thinner sheaths and more sheath curvature. The sheath curvature at the edge of the wafer contributes to skewing ion trajectories and producing a tilt. Plasma properties that thin the sheath over the wafer and FR properties that thicken the sheath over the FR reduce sheath curvature and so lessen ion tilt at the edge of the wafer.

The model used in this investigation and reactor conditions are described in Sec. II. Plasma properties for the base case are discussed in Sec. III. Consequences of varying the bias frequency and FR properties on edge exclusion and ion tilt are discussed in Sec. IV. Concluding remarks are in Sec. V.

II. DESCRIPTION OF THE PLASMA REACTOR MODEL

The simulation of plasma dynamics was performed using the Hybrid Plasma Equipment Model (HPEM) described in detail in Refs. 24 and 25. A brief summary is given here. The HPEM is a two-dimensional (2D) hydrodynamics model using modules containing unique physics that exchange physical quantities with other modules. These quantities include, for example, electric and magnetic fields, densities of charged and neutral species, particle distribution functions, and rate coefficients for electron impact processes. The main modules used in this work are the Electromagnetics Module (EMM), Fluid Kinetics-Poisson Module (FKPM), Electron Energy Transport Module (EETM), and Plasma Chemistry Monte Carlo Module (PCMCM).

The amplitude and phase of electromagnetic fields produced by the antenna (coils) and absorbed in the plasma are computed in the EMM using a frequency domain solution of the wave equation. The FKPM integrates continuity, momentum, and energy equations, solving for neutral and charged heavy particle densities, fluxes, and temperatures. Poisson's equation is solved simultaneously with continuity equations for charged particles which provide surface and volume charge densities, needed to produce the electrostatic potential. The fluid-treated bulk electron flux is obtained from a Scharfetter–Gummel drift-diffusion model, also within the FKPM. Transport and rate coefficients for bulk electrons are produced from electron energy distributions (EEDs) obtained from solutions of stationary Boltzmann's equation using a two-term spherical harmonic solution. EEDs for sheath accelerated electrons produced by secondary emission by ions were calculated using a kinetic Monte Carlo method in the EETM using electric fields produced the FKPM and electromagnetic fields from the EMM. Electron impact rate and transport coefficients were then produced from the EEDs for use in the FKPM. Ion trajectories onto the substrate or other surfaces are tracked in the PCMCM using Monte Carlo methods. The result is energy and angular distributions (IEADs) onto the wafer as a function of position on surfaces.

The DC bias on the substrate, V_{DC}, is calculated as follows.[24] The total current collected by the powered electrode is computed by performing an integral over its surface area of the sum of conduction current density and displacement current density. A similar integral is performed for current collected by metal surfaces on the grounded side of the circuit. These currents are then used to charge a blocking capacitor placed between the power supply and powered electrode. If these two currents are not equal, then there is a net charge placed on the capacitor and generation of V_{DC}. The charging process and V_{DC} naturally come to a steady state when the currents on the powered and grounded sides of the circuit are equal.

Simulations were performed for ICPs sustained in $Ar/Cl_2/O_2$ gas mixtures as commonly used for plasma etching of DTI structures. The Ar/Cl_2 and Ar/O_2 portions of the reaction mechanism are the same as discussed in Refs. 26 and 27. Reactions between Cl and O species are described in Ref. 28.

A schematic of the cylindrically symmetric ICP reactor used in this work is in Fig. 1. The reactor is powered by a flat four-turn antenna (coils) above an alumina dielectric window 1.5 cm thick and with a relative permittivity of $\varepsilon/\varepsilon_0 = 9.85$. The window also serves as the gas injection shower head. The spacing between the window and wafer is 19.4 cm. The 300 mm diameter wafer (nominal dielectric constant $\varepsilon/\varepsilon_0 = 12.5$ and conductivity $0.01\ S\ cm^{-1}$) sits on the lower metal electrode surrounded by an alumina focus ring having a width of 3.75 cm and conductivity of $10^{-6}\ S\ cm^{-1}$. Electrically, the capacitance of the wafer dominates. To achieve the electrical capacitance corresponding to a wafer thickness of 775 μm, the permittivity of the wafer material is adjusted so that the appropriate capacitance results with the available mesh resolution. Gas pumping is through an annular port surrounding the focus ring having a width of 5.1 cm, providing an internal diameter of the chamber of 47.6 cm. The outer walls of the chamber are grounded metal. Secondary electron emission coefficients due to ion impact for materials in direct contact with

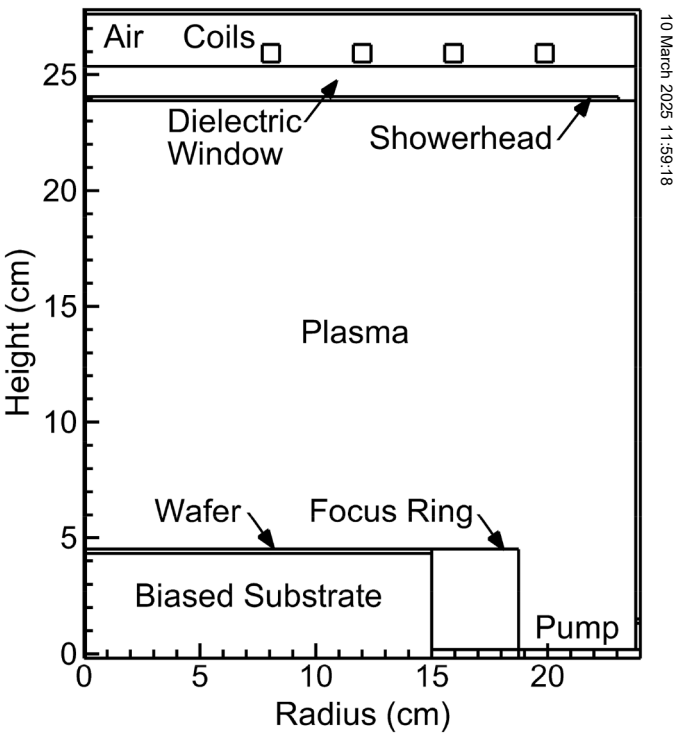

FIG. 1. Schematic of the ICP reactor. The biased substrate is connected to the RF power supply through a blocking capacitor.

the plasma were 0.15, 0.10, and 0.02 for the wafer, dielectrics, and metals.

The wafer in this investigation is modeled as pure silicon when in practice the wafer would have on its plasma facing surface patterned photoresist and underlying dielectric layers. These layers are very thin (typically less than a few micrometers), which translates to a large capacitance and small impedance. The voltage dissipated by these layers is proportionally small and has little effect on IEADs incident onto the wafer. Any surface charging from the thin dielectric layers typically has little impact on the surface potential compared to the RF sheath.[29,30]

In order to isolate the consequences of the electrical properties of the FR on IEADs, the wafer and focus ring height are equal with there being no gap between the wafer and FR. These conditions will reduce possible geometrical influences on sheath properties. Previous work has shown that the relative heights of the FR and wafer, and width of the wafer-FR gap, produce sheath curvature that can either contribute to or correct ion tilt.[19,20] The trends addressed in this study are expected to apply for different wafer and FR layouts.

The feedstock gas $Ar/Cl_2/O_2 = 90/9/1$ was supplied at 300 SCCM through the showerhead at the top of the reactor. The pressure was held constant at 15 mTorr at the entrance to the pump.

The bias power supply was connected to the lower electrode through a blocking capacitor. For the system to reach quasisteady state, the DC self-bias must also reach steady state for a given RC time constant for the blocking capacitor. To shorten the time required for the blocking capacitor to charge, its capacitances was varied from 10 to 100 nF over a time of 5 μs. The blocking capacitance was held at 100 nF for the remainder of the simulation. The DC self-bias, V_{DC}, may oscillate during a VLF period if the RC time constant for the blocking capacitor is commensurate with the RF period.[31,32]

The charging of the blocking capacitor results from there being a difference in charge delivered to the capacitor from the grounded and powered sides of the circuit. The current to the capacitor on the grounded side of the circuit consists of conduction and displacement current flowing to the walls of the plasma chamber, and displacement current flowing to the top of the chamber through the dielectric window. Current flowing through the powered side of the circuit consists of conduction and displacement current flowing through the wafer, and displacement current flowing through the focus ring. With the displacement current components of the bias currents being functions of bias frequency, the final values of V_{DC} are functions of bias frequency.

The IEADs discussed here are time averages of the total ion flux consisting of Ar^+, Cl_2^+, Cl^+, O_2^+, and O^+ onto the wafer during the RF period. Electric fields are recorded as a function of position and phase in the FKPM over an RF period. Those fields and source functions are used to launch and track the trajectories of particles in the PCMCM that then strike the wafer, which are then recorded to produce the IEADs as a function of position on the wafer. The basic structure of the HPEM is to iterate through different physics models exchanging information between the modules with a period of τ_E which is typically 0.5–1 μs. When operating with a VLF bias, the RF period, τ_{RF}, may exceed τ_E which then violates the hierarchy for data exchange between modules. To address these conditions, a low frequency option was developed that enables recording of electric fields over several τ_E exchange periods and so enables computation of IEADs for VLF biases.

III. PLASMA PROPERTIES

The base case plasma conditions are a $Ar/Cl_2/O_2 = 90/9/1$ gas mixture at 15 mTorr, with a flowrate of 300 SCCM, ICP power of 500 W at 10 MHz, with a 1 MHz bias on the substrate having a constant 1 kV voltage amplitude. The electron density, power deposition, and ionization source are shown in Fig. 2 for the base case. The electron density is maximum at 7.2×10^{10} cm^{-3}, with the ratio of ion densities being $Cl_2^+/Ar^+/Cl^+/O_2^+/O^+ = 80/13/6/1/0.03$. In addition to the mole fractions which favor ionization of Ar and Cl_2, a charge exchange cascade (Ar^+, Cl^+, and O^+ having the higher ionization potentials) favors formation of Cl_2^+. The cycle average sheath width above the powered substrate is 0.95 cm, decreasing to 0.19 cm at the edge of the FR. This change in width of the sheath results in sheath curvature over the edge of the wafer.

It is industrial practice in developing processes to control bias power as opposed to controlling bias voltage. In this parametric study, we are instead controlling bias voltage and FR properties while not holding bias power constant. The goal of this investigation is to quantify the consequences on IEADs of FR properties. Controlling voltage enables changes in IEADs due to FR properties to be more clearly defined. Keeping bias power constant when varying source power, bias frequency or focus ring characteristics requires a simultaneous change in the bias voltage, which would make comparing the IEADs more difficult.

Power deposition from the ICP source delivering 500 W is maximum as 0.23 W/cm^3, centered under the antenna. The power deposition by capacitive coupling includes both ion accelerating through the sheath and stochastic sheath heating of electrons. For a 1000 V voltage amplitude and a V_{DC} of −750 V, bias power is maximum at 1 W/cm^3 with a total power deposition of 1.5 kW.

The ionization source by bulk electrons closely follows that of the ICP power deposition, with a maximum value of 2.6×10^{15} cm^{-3}s^{-1}. Ionization by sheath accelerated secondary electrons has a maximum value of about 1/10 that of the bulk (1.5×10^{14} cm^{-3} s^{-1}). The secondary electrons produce an electron-beamlike source that has two components. The first component results from electrons accelerated perpendicularly away from the wafer covered electrode, which indicates that the sheath is fairly parallel to the wafer. Such a parallel sheath would produce ions onto the substrate which arrive with near normal angles. The second component of the electron beam results from secondary electrons that are accelerated with a non-normal angle from the edge of the wafer and from over the FR. These off-normal electron beams result from sheath curvature across the edge of the wafer and FR [see Fig. 2(a)], which is a topic of the following discussion.

IV. CONSEQUENCES OF BIAS FREQUENCY AND FR PROPERTIES ON IEADS AT THE EDGE OF THE WAFER

Electron densities for bias frequencies of 250 kHz and 5 MHz are shown in Fig. 3. The maximum plasma density does not significantly change between the high bias frequency of 5 MHz and the low bias frequency of 250 kHz. The plasma density is primarily

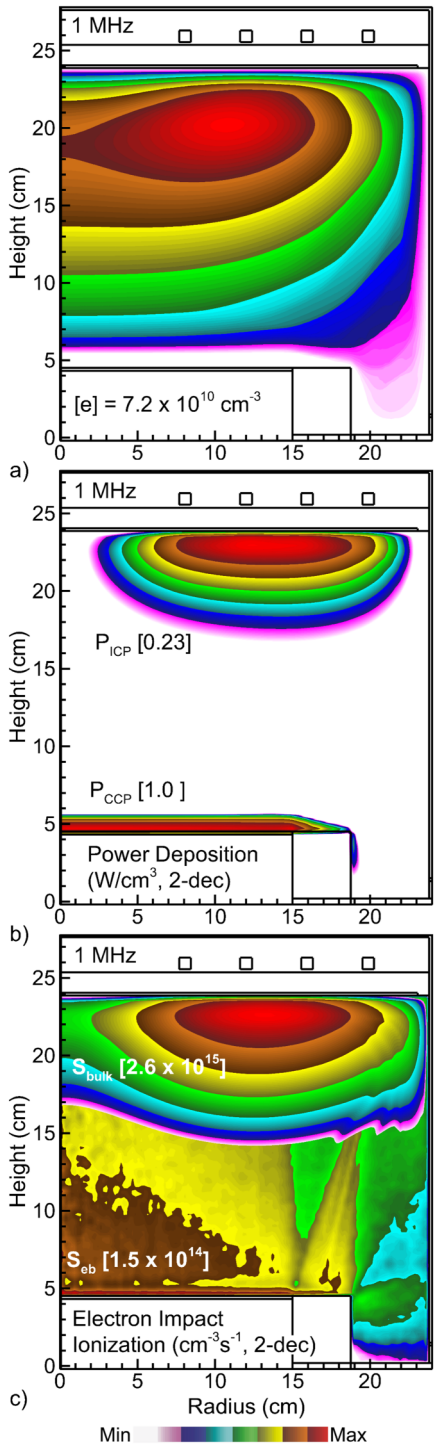

FIG. 2. Properties for the base with a 1 MHz bias. (a) Electron density, (b) power deposition, and (c) ionization source. S_{bulk} is the ionization by bulk electrons. S_{eb} is the ionization by sheath accelerated secondary electrons. The maximum value is noted in each image with the range of decades for log plots.

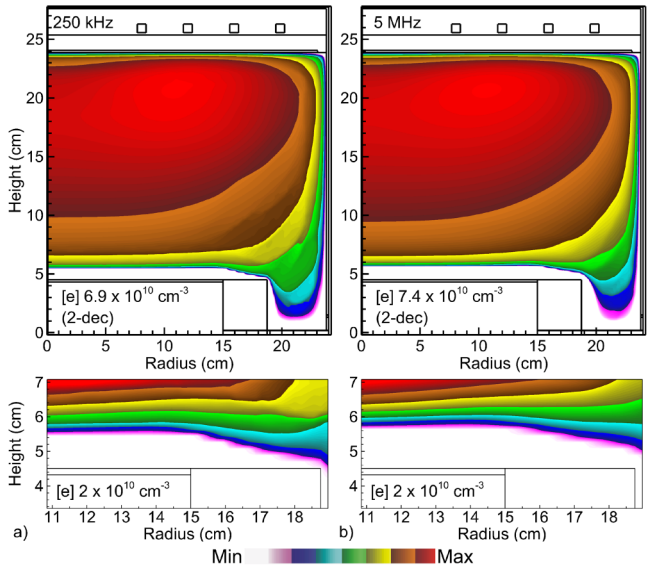

FIG. 3. Electron density at the peak cathodic (most negative) part of the RF cycle for (a) 250 kHz and (b) 5 MHz. The lower images are enlargements of the sheaths at the edge of the wafer and over the FR. The maximum value in each image is noted with the range of decades for log plots.

determined by the ICP power deposition with the majority of the bias power being dissipated by ion acceleration in the sheath. However, with sheath heating of electrons being proportional to the square of the bias frequency, there is non-negligible electron heating at the higher bias frequency. This increase in electron heating produces a local source of ionization above the sheath that results in a small increase, about 5%, in the maximum plasma density at 5 MHz as compared to 250 kHz. This increase in plasmas density produces small changes in sheath thickness over the wafer. However, the most significant change in sheath properties is over the FR. At 250 kHz, the sheath edge is sloped over the entire width of the FR. At 5 MHz, the slope of the sheath edge over the FR is significantly reduced. These trends largely result from the charging and discharging of the capacitance of the FR.

Current flowing through the blocking capacitor and the biased electrode has two paths to the plasma. The first current path is through the wafer and is limited by the series impedance of the wafer and the sheath bounding the wafer. The second path is through the FR and is limited by the series impedance of the FR and the sheath bounding the FR. The FR impedance is dominated by its capacitive reactance. The RC time constant we refer to below is the time required to charge the capacitance of the FR by current collected on the surfaces of the FR. When fully charged, the FR will have a voltage essentially equal to the sheath potential that would form above the conductive wafer. This RC charging time is distinct from the charging time of the blocking capacitor as the current flowing into the blocking capacitor has contributions from current flowing through the wafer.

Current flowing from the plasma through the sheath above the FR and into the electrode passes through the FR as displacement current. However, as would a capacitor, the low conductivity FR charges as a result of conduction current from the plasma terminating at its surface. The impedances of the sheath and FR are large compared to the bulk plasma, and so the majority of the applied voltage is dropped across the sheath and the FR. These impedances are dominated by their reactive capacitance with the smaller capacitance (larger impedance) dissipating the larger voltage.

When decreasing the bias frequency, the impedance of both the sheath and the FR increase as the capacitive reactance scales as $1/(\omega C)$, with C being the capacitance of either the sheath or FR and ω being the RF radian frequency. With there being little change in ion fluxes onto the FR and bulk plasma impedance with changes in bias frequency, the rate of charging of the capacitance of the focus is nearly the same while the RC time constant for charging the FR, τ_{RC}, does not change. At 250 kHz, the RF cycle, 2.5 μs, is commensurate with τ_{RC} and so the FR nearly fully charges. This charging of the FR removes voltage from the sheath to the extent that at the outer edge of the FR, there is essentially no sheath. The slope in the edge of the sheath results from the differential charging of the FR, as the voltage to which the FR charges is a function of radius. At 5 MHz, the RF cycle is 0.2 μs which is shorter than τ_{RC}. As a result, the FR does not fully charge. Voltage is then divided between the capacitance of the FR and the capacitance the sheath. The oscillation of the finite thickness sheath produces displacement current that subsequently flows through the uncharged capacitance of the FR. The end result is a less steep slope of the sheath across the edge of the wafer and the FR.

These trends can also be viewed in terms of local voltage division of the series impedances between the powered electrode and the plasma. The FR and sheath above the FR are impedances in series. With the impedance of the FR being essentially purely capacitive and increasing with decreasing frequency, a larger proportion of the voltage between the powered electrode and plasma is dropped across the FR, leaving less voltage across the sheath which then thins the sheath. Since the distance along an electric field line between the electrode and the surface of the FR increases with increasing radius of the FR, the capacitance along this field line decreases. The decreasing capacitance increases the impedance and voltage drop across the radius of the FR. Proportionately, less voltage is then available for the sheath at large radius on the FR, leading to a thinner sheath.

The differences in curvature of the sheath with bias frequency are shown by the plasma potentials in Fig. 4 for bias frequencies between 250 kHz and 5 MHz at the peak of the cathodic (most negative) portion of the RF cycle. The curvature of the sheath occurs at the edge of the wafer where the sheath transitions from being parallel over the wafer to being sloped over the FR. The curvature of the sheath extends over the outer few millimeters of the wafer, leading to edge exclusion.

For a collisionless, one-dimensional sheath, ions entering the sheath will be accelerated into the wafer in a direction that is initially perpendicular to the sheath edge. A slope to the sheath will result in ions arriving at the wafer with a non-normal angle. (An incident angle of 0° is normal to the surface.) With extension over the wafer

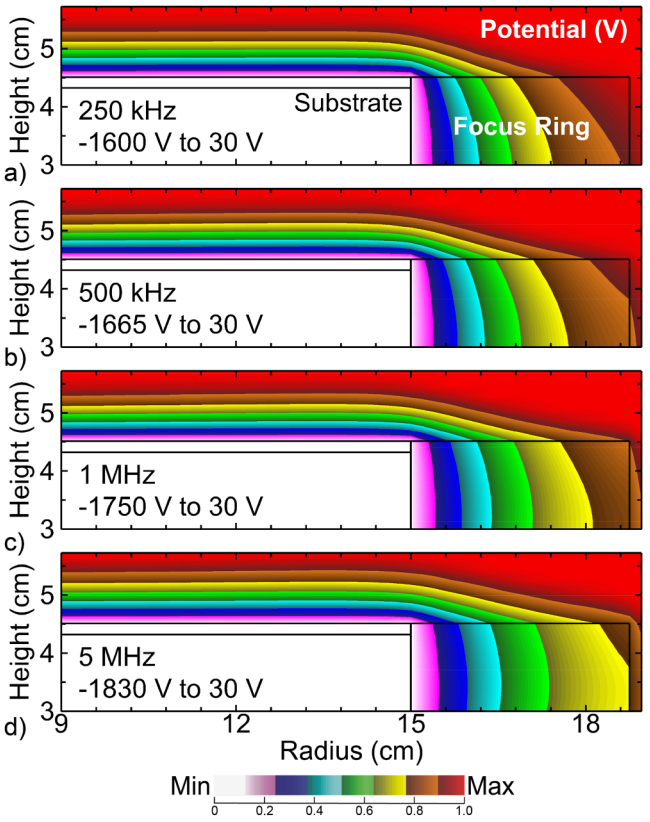

FIG. 4. Electric potential at the peak cathodic (most negative) part of the RF cycle for substrate bias frequencies of (a) 250 kHz, (b) 500 kHz, (c) 1 MHz, and (d) 5 MHz. The range of potential in each image is noted.

of the nonparallel sheath edge (sheath curvature), ions will strike the wafer at non-normal angles.

While FR charging plays a major role in the width and curvature of the sheath across the FR, electron sheath heating and local ionization can also alter the slope of the sheath.[33,34] At higher bias frequencies, there is more electron sheath heating and more local ionization sources. Discharges with bias frequencies of ≥1 MHz are predominately in a stochastically heated mode due to the large sheath voltage.[35,36] The ionization source at the top of the reactor is dominantly due to the inductively coupled power. This ionization source is largely independent of the bias frequency, as the plasma density is large enough to shield the voltage bias voltage oscillations from the bulk plasma. With the dielectric window adjacent to the ICP power deposition being an electrically floating surface, the surface of the window rapidly charges to the floating potential, thereby limiting sheath oscillation and local heating.

The DC self-bias voltage increases in magnitude, becoming more negative with increase in bias frequency, as shown in Fig. 5. V_{DC} decreases from −600 V at 250 kHz to −850 V at 5 MHz, for an applied bias voltage amplitude of 1000 V. These voltages produce bias powers of 590 W at 250 kHz and 560 W at 5 MHz. A more

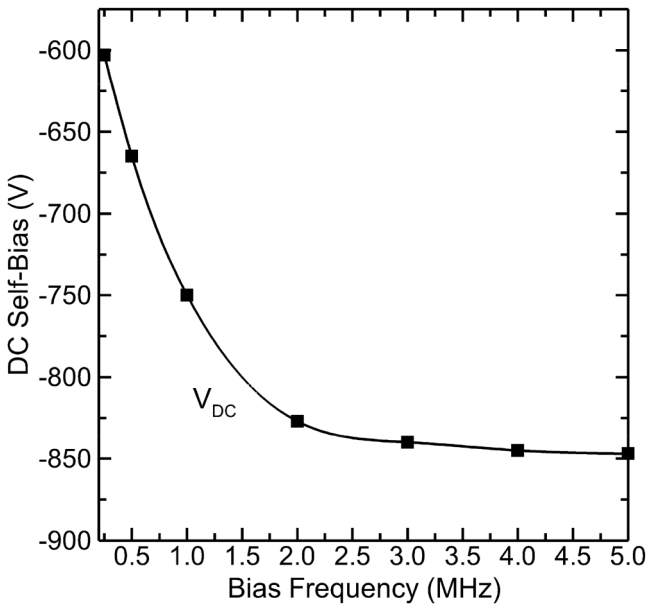

FIG. 5. DC self-bias voltage as a function of bias frequency.

negative V_{DC} indicates that the powered substrate appears to be a smaller collector of current than grounded surfaces. V_{DC} becomes more negative to increase current collection on the powered substrate so that the net charge collected per cycle on the powered electrode to be equal that of the grounded electrode.

The trend of a less negative V_{DC} for lower frequencies is counter-intuitive if the V_{DC} is dominated by current flowing through the FR. Decreasing frequency produces a higher impedance of the FR resulting in less current flowing through the FR to the substrate which would produce a more negative V_{DC}. The value of V_{DC} is determined by the difference in current flowing to the powered and grounded sides of the circuit. For ICP reactors, the return path to ground for the bias current includes the side walls of the reactor and current flowing through the top dielectric window to grounded surfaces above the window. With the top dielectric window having a negligible conductivity, the majority of current passing through the window is displacement current. The displacement current through the window increases with increasing frequency. The current collected by the powered electrode has a large proportion of conduction current through the wafer, which depends weakly on frequency. As a result, current collection between powered and grounded surfaces becomes less balanced with increasing frequency, which then results in a more negative V_{DC} with increasing frequency.[31,32,37]

The ion plasma frequency is approximately 1 MHz for an ion density of 2×10^{10} cm^{-3} and mass of Cl_2^+, the dominant ion. Lighter ions (such as O^+ and Ar^+) respond to bias frequencies of roughly between 100 and 700 kHz; however, their lower densities result in smaller contributions to the IEADs onto the wafer. IEDs are often characterized by the ratio of the ion transit time to the RF period,[12]

$$S = \frac{\tau_{ion}}{\tau_{rf}} = \bar{s}\nu_{rf}\left(\frac{2M}{q\overline{V}_s}\right)^{1/2}. \quad (1)$$

The sheath transit ratio, S, of the ion traversal time, τ_{ion}, over the rf period, τ_{rf}, determines the frequency regime the sheath is in. $\bar{s}$ and $\overline{V}_s$ are the mean sheath width and mean sheath voltage where the bias frequency is ν_{rf} and M is ion mass. Values of $S \ll 1$ are the thin-sheath limit where ions are accelerated across the sheath in times short compared to the RF period and, for collisionless sheaths, arrive on the wafer with an energy corresponding to the instantaneous sheath potential. This results in broad, double peaked (low and high energy) IEDs. Values of $S \gg 1$ are the thick sheath limit where ions require many RF periods to cross the sheath and arrive on the wafer with an energy corresponding to the average sheath potential. For collisionless conditions, this results in narrow IEDs with low and high energy peaks converging toward the average. For our conditions, at 1 MHz, $S \approx 0.5$, which is approximately the boundary between the thin sheath, low frequency regime and the thick sheath, high frequency regime.

The angle integrated ion energy distributions (IEDs) averaged over the wafer for frequencies from 250 kHz to 5 MHz are shown in Fig. 6. IEDs for all frequencies are double peaked, with the expected convergence at high frequencies toward a single peak with an average energy being the DC bias. As frequencies decrease, the minimum energies decrease and maximum energies increase. However, with the decrease in magnitude of the V_{DC} at low frequencies, the maximum ion energy saturates.

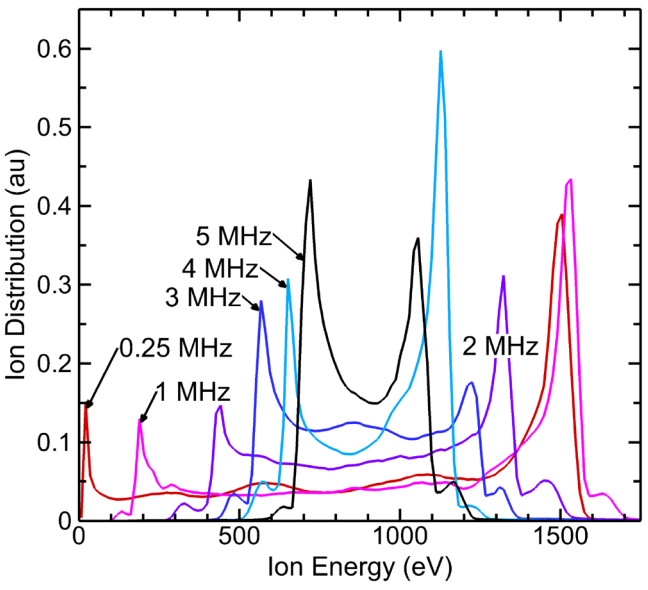

FIG. 6. Ion energy distributions (IEDs) averaged across the entire wafer for bias frequencies ranging from 250 kHz to 5 MHz.

Several factors determine the slope and curvature of the sheath as a function of radius over the wafer and bias frequency, and particularly so approaching the edge of the wafer. One component of that dependence is the charging of the FR, producing more sheath curvature at lower frequencies. IEADs incident onto the wafer averaged for all ions (though dominated by Cl_2^+) for bias frequencies of 250 kHz and 5 MHz are shown in Fig. 7 at radial locations approaching the edge of the wafer. Here, positive angles represent ion trajectories slanted toward the center of the wafer (left) and negative angles represent ion trajectories slanted toward the chamber wall (right).

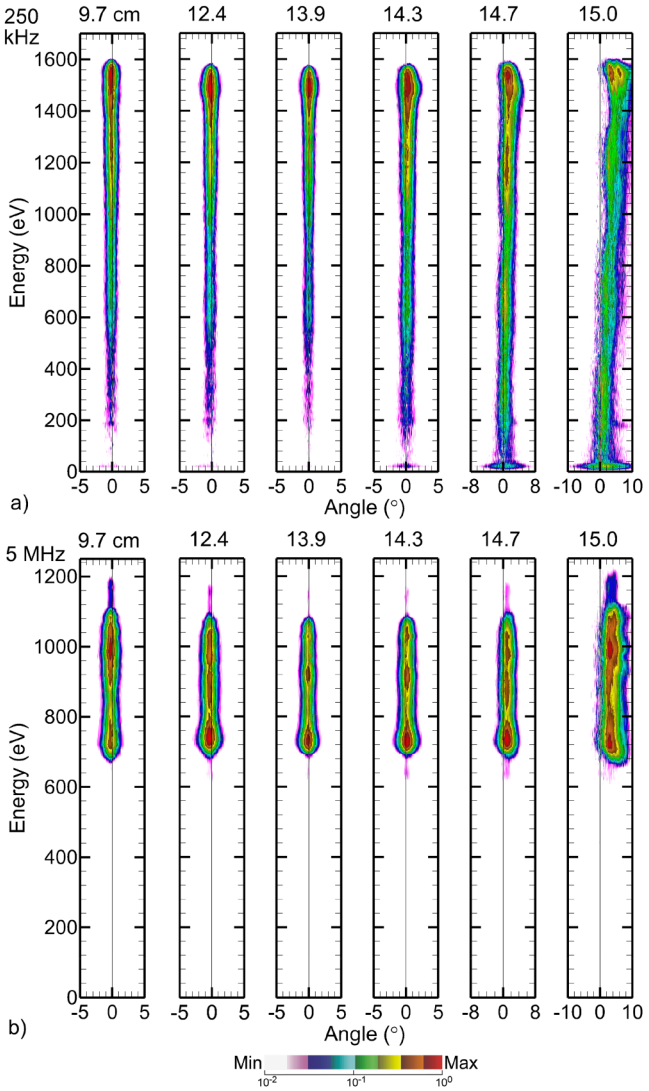

FIG. 7. Ion energy and angular distributions (IEADs) at radial positions approaching the wafer edge for bias frequencies of (a) 250 kHz and (b) 5 MHz. Note that the range of angles plotted increase approaching the edge of the wafer. The images are plotted on a two-decade log scale.

With the wafer being 15 cm in radius, 9.7 cm is at about 2/3 of the wafer radius. At this radius, the sheath is largely parallel to the wafer at all frequencies, and ion trajectories are nearly normal to the wafer. The IEAD at 250 kHz extends to both smaller and larger energies, consistent with being in the thin-sheath limit. IEADs approaching the edge of the wafer (15 cm) are displayed with a larger range of angles as the trajectories of the ions are diverted significantly from the normal by sheath curvature. With the RF period being long enough to charge the FR, the sheath potential above the FR at 250 kHz is significantly smaller than above the wafer, producing a thinner sheath and sheath curvature across the edge of the wafer. This sheath curvature results in a progressively more tilted IEAD approaching the edge of the wafer. The ions within the IEAD that have the largest tilt also have the largest energies. These most tilted ions originate from ions entering the sheath at the maximum cathodic portion of the cycle when the sheath is thickest. These trends indicate that the most severe sheath curvature occurs at the peak of the cathodic portion of the cycle.

The IEADs as a function of radius for 5 MHz have the expected narrower energy spread with similar near-wafer-edge tilting of the distribution. The tilting, however, is less severe with a bias of 5 MHz than at 250 kHz. The tilting is largely limited to the very edge of the wafer. With the shorter period at 5 MHz and less charging of the FR, the sheath potentials above the wafer and above the FR have commensurate values, producing more similar sheath widths and so less curvature in the sheath. The end result is there being less tilt in the IEAD approaching the edge of the wafer. The tilt within the IEAD at 5 MHz is nearly uniform as a function of energy. With the time needed for the ion to cross the sheath being many RF periods, the IEADs reflect an average of not only the sheath potential but also an average of the sheath curvature. Ions of all energies, therefore, have a similar tilt.

The energy integrated ion angular distributions (IADs) striking the wafer at different radii are shown in Fig. 8 for bias frequencies of 5 MHz and 250 kHz. The angular width and tilt of the IADs are summarized in Fig. 9. The IADs for 250 kHz at radii <14.3 cm are generally normal to the wafer with a uniform angular width, indicating a fairly uniform and flat sheath. For radii >14.3 cm, the IADs have a progressively larger positive tilt with the IAD broadening. The IADs for 5 MHz show a similar trend through with less severe positive tilt at the edge of the wafer. The IADs for 5 MHz have a small negative tilt at radii <12.4 cm. This reversal of the tilt results from a global curvature of the sheath across the wafer, having a minimum in curvature at about 12–13 cm. The sheath has a minimum thickness at this location due to a local maximum in plasma density. This local maximum is likely related to the localized electron sheath heating at the higher frequency.

The trends for angular width and tilt (Fig. 9) are summarized as follows. Lower bias frequencies (several hundred kHz) generally produce IEADs having smaller angular spread and less asymmetry (smaller tilt), with more uniformity across the wafer. Approaching the focus ring, both angular spread and tilt increase. Higher bias frequencies (several MHz) produce IEADs having larger angular spread with asymmetries that may vary across the wafer. The increases in angular spread and tilt approaching the FR for higher frequencies will generally be smaller than for lower frequencies.

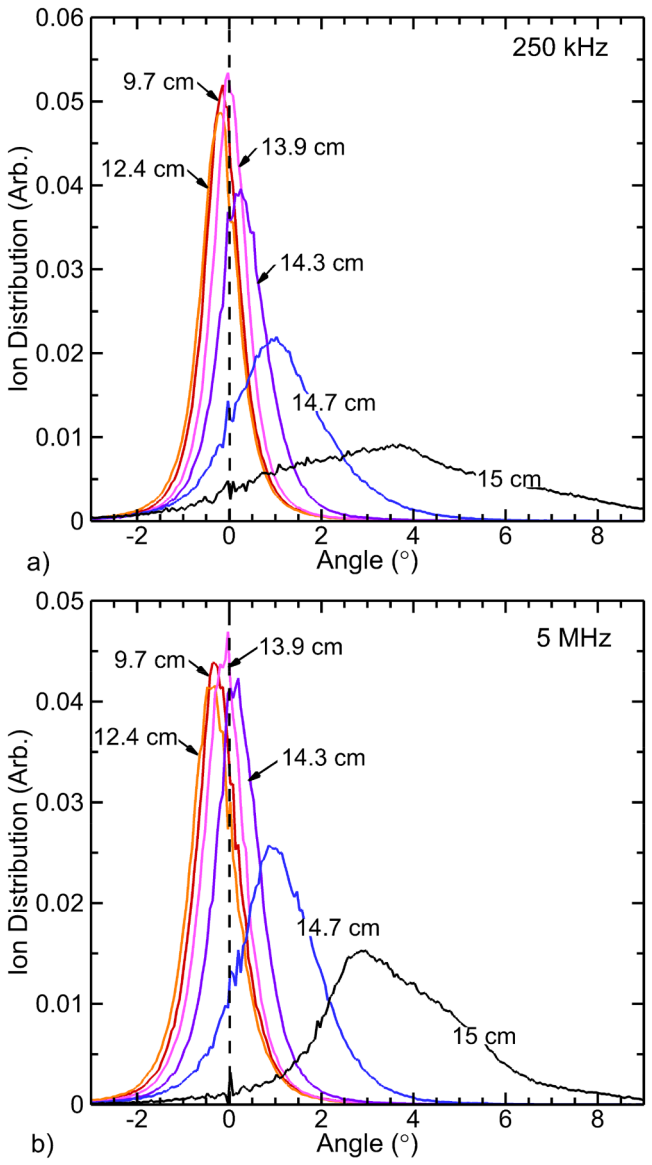

FIG. 8. IADs at radial positions approaching the wafer edge for bias frequencies of (a) 250 kHz and (b) 5 MHz.

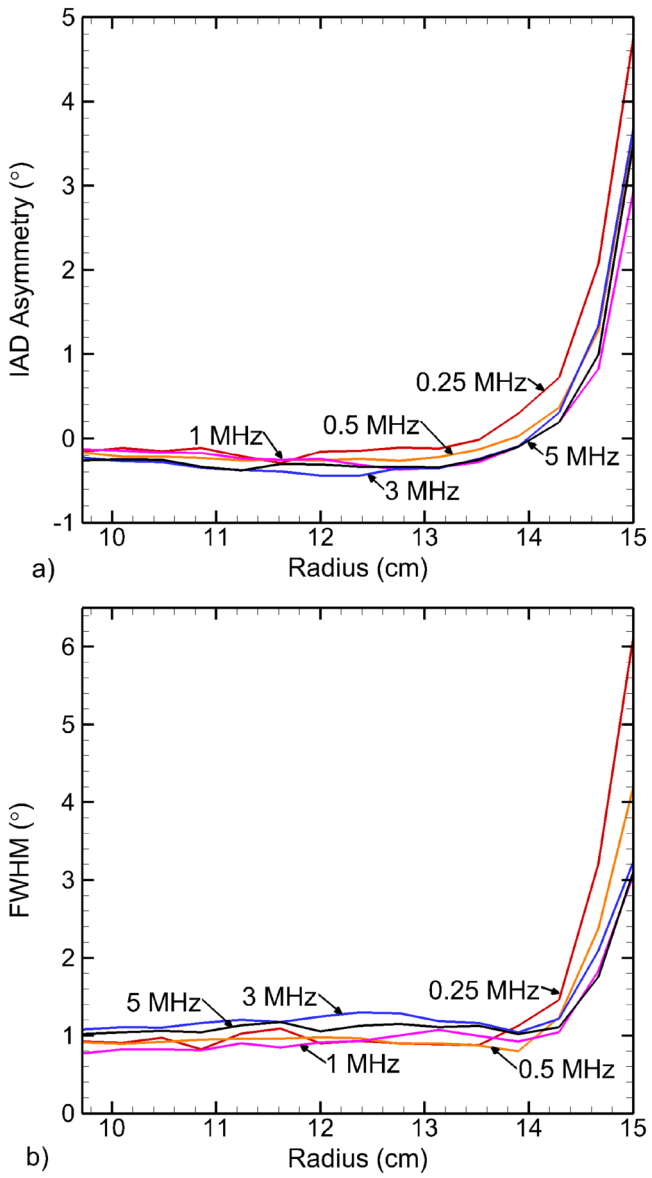

FIG. 9. Angular properties of the IEADs as a function of radius for different bias frequencies. (a) IAD asymmetry (tilt) and (b) angular full width half maximum (FWHM).

These trends are largely explained by sheath curvature and FR charging. As such, reactor parameters that affect FR charging will also affect the tilt and angular breadth of IEADs approaching the FR. These parameters include bias power, ICP (source) power, and permittivity (dielectric constant) and conductivity of the FR. Another parameter that can impact FR charging is the secondary electron emission (SEE) coefficient by ion bombardment of the FR. A parametric study of the SEE coefficient of the FR was performed over the range of 0.01–0.25. Increasing values of SEE moderately increased the ion asymmetry at the wafer edge from 3.2° to 3.4° (radii >14.7 cm), due to there being a larger gradient of surface charging across the FR. The SEE coefficient of the FR is sensitive to, for example, surface roughness that may vary as the FR erodes.[38] This variability in surface charging due to the drift in SEE coefficient would then lead to a drift over time of the IEADs at the wafer edge.

The amplitude of the bias voltage was varied from 500 V to 5 kV for otherwise the base case conditions. The resulting IEADs at the edge of the wafer for 250 kHz and 5 MHz bias frequencies are

shown in Fig. 10. The electric potentials in the vicinity of the wafer edge at bias frequencies of 250 kHz and 5 MHz for bias voltages of 500 V and 5 kV are shown in Fig. 11 at the peak of the cathodic portion of the cycle. Varying the voltage from 500 V to 5 kV produces bias powers of 310 W to 12.1 kW at 250 kHz and 190 W to 12.0 kW at 5 MHz. The plasma density at the sheath edge remains fairly constant with change in bias voltage. As a result, with increasing bias voltage the sheath thickness increases. From 500 V to 5 kV, the sheath thickness increases from 0.76 to 1.9 cm at 250 kHz and 0.58 to 1.5 cm at 5 MHz. With mean-free paths being commensurate to or exceeding these dimensions, particularly at higher energies

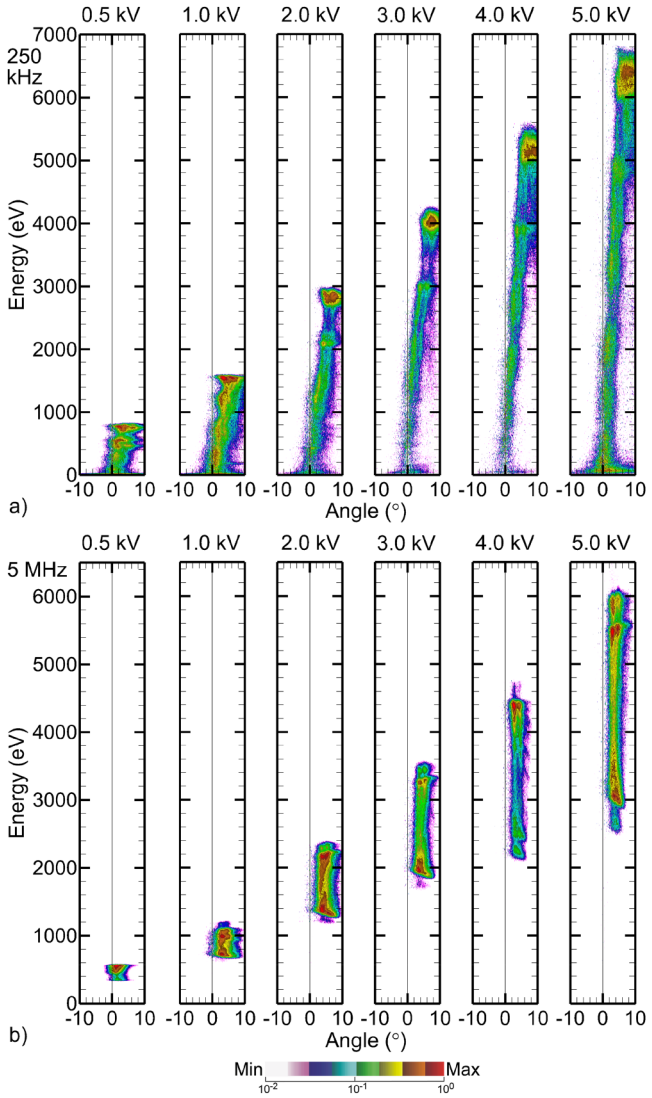

FIG. 10. Ion energy and angular distributions (IEADs) at the edge of the wafer for bias voltages of 0.5–5 kV for bias frequencies of (a) 250 kHz and (b) 5 MHz. The images are plotted on a two-decade log scale.

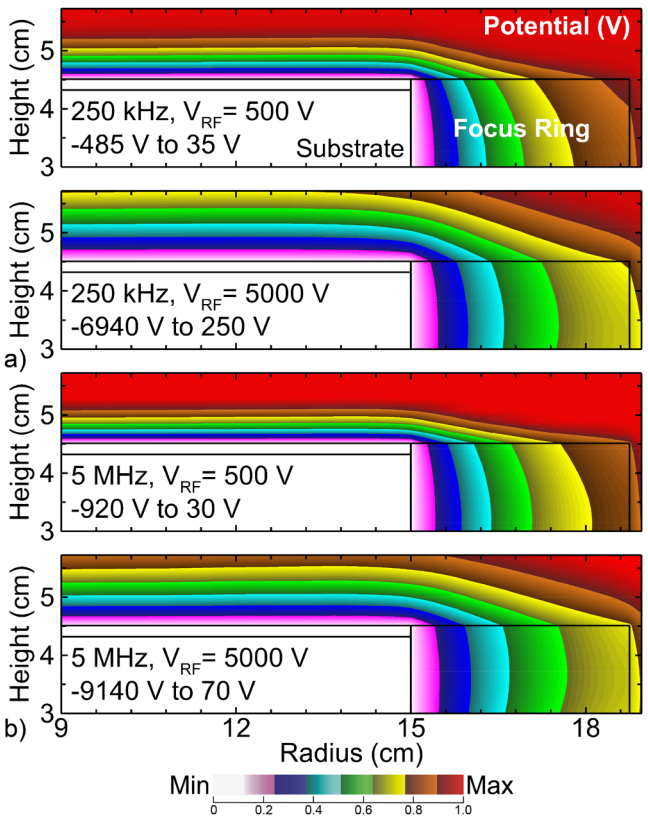

FIG. 11. Electric potential at the peak cathodic part of the RF cycle for bias frequencies of (a) 250 kHz and (b) 5 MHz for 500 V and 5000 V bias voltage. The ranges of potential in each image are noted.

where elastic collision cross sections decrease, ion transit through the sheath is largely collisionless.

The angular tilt and breadth of the IEADs uniformly increase with increasing bias voltage in approaching the FR. This increase in tilt is due in large part to the thickening of the sheath which increases its curvature. The degree of tilting increases with ion energy, a consequence of the high energy ions entering the sheath at its maximum extent when curvature is also most extreme. This increase in tilt with increasing voltage is more severe for a bias frequency of 250 kHz, as at 5 MHz, ions require several RF periods to cross the sheath, and so respond to an average curvature of the sheath. With the ion current to the substrate being essentially constant, the charging of the FR takes a larger fraction of the RF cycle with increasing voltage. At 250 kHz, the charging time remains shorter than the RF cycle. At 5 MHz, the increase in charging time is commensurate with the RF cycle, thereby mildly lessening the tilt of the IEAD at high voltage.

For a given frequency and constant bulk plasma density, increasing bias voltage thickens the sheath and so increases sheath speed. This increase in sheath speed increases the rate of stochastic heating of the electrons at the edge of the sheath. This stochastic

heating leads to a higher rate of ionization adjacent to the sheath. Although ionization is dominated by the ICP source power, this local increase in ionization does add to the plasma density, leading to a small decrease in sheath thickness. Although the goal of high plasma density systems, such as ICPs with a substrate bias, is to separate the production of ion fluxes from their acceleration into the wafer, there will be a bias voltage above which this goal is violated and that will affect sheath curvature. Since the discontinuity in sheath heating is greatest at the edge of the wafer, any perturbation in ionization sources will affect sheath curvature, either for benefit or not for benefit.

The angular tilt and angular spread of IADs approaching the edge of the wafer are shown in Fig. 12 for bias frequencies of 250 kHz and 5 MHz for bias voltages of 500 V to 5 kV. The general trend is an increase in IAD asymmetry (tilt) with increasing bias voltage, with the increase in tilt starting at smaller radii as the

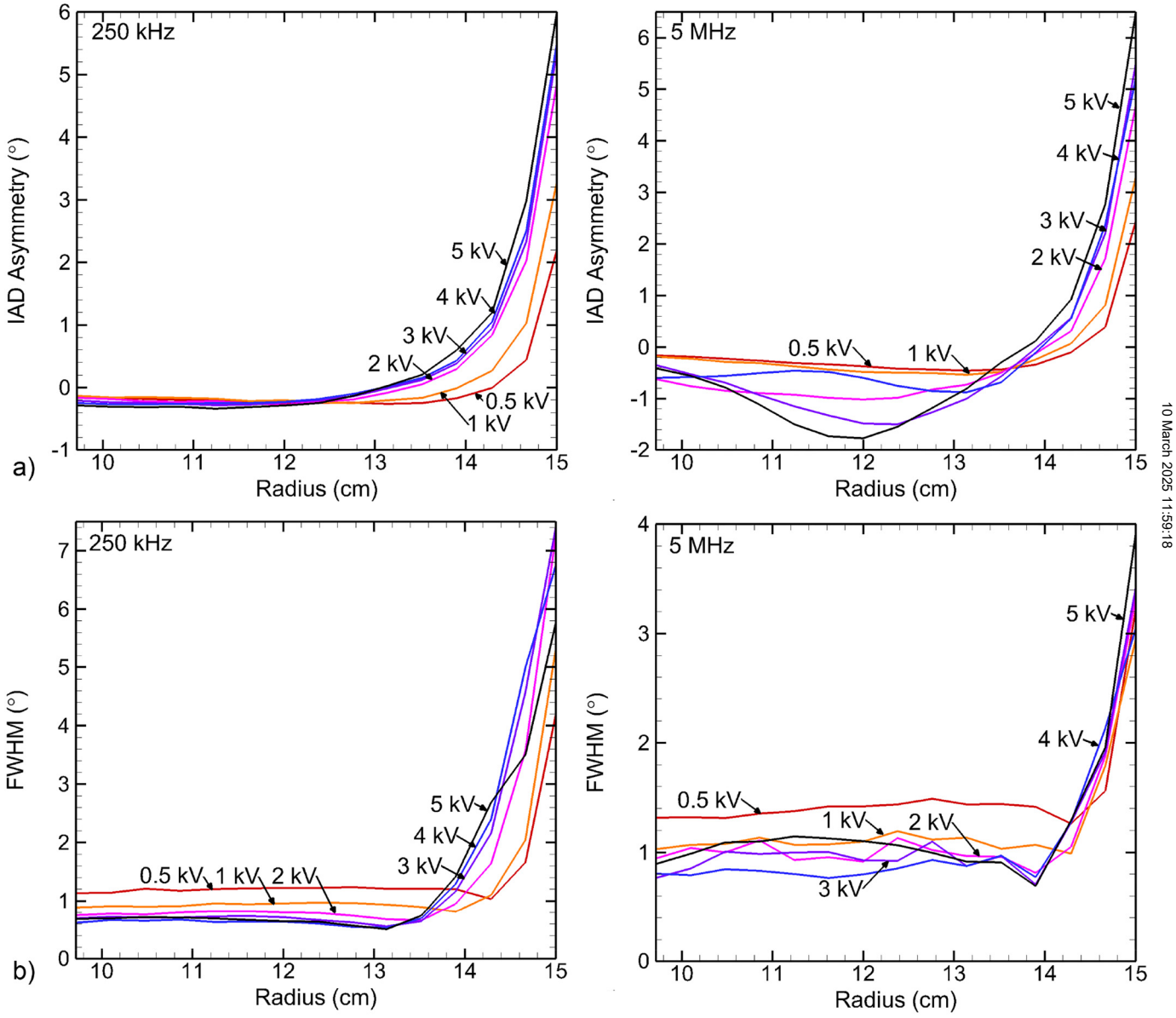

FIG. 12. Angular properties of the IEADs as a function of radius for bias voltage amplitudes of 0.5–5 kV. (a) IAD asymmetry (tilt) for bias frequencies of 250 kHz and 5 MHz and (b) FWHM for 250 kHz and 5 MHz.

voltage increases. This trend would imply an increasing amount of edge exclusion with increasing voltage. At 250 kHz, the asymmetry over the center of the wafer is insensitive to voltage. At 5 MHz, asymmetry over the wafer worsens with increase in voltage, producing a reversal in the tilt (from inwardly pointing to outwardly and back to inwardly). This trend results from sheath heating producing local ionization and a local increase in plasma density. This increase in plasma density locally thins the sheath, which modulates the curvature of the sheath. These results should be interpreted qualitatively. They indicate that any perturbation in the curvature of the sheath translating into a tilt of the IEAD can be amplified with large bias voltages. These results do align with anecdotal evidence of the tilt of HAR features reversing and recovering at the middle of the wafer.

The motivating principle of two-frequency capacitively coupled plasmas is that the high frequency controls the plasma density and the magnitude of the ion flux onto the wafer, while the low frequency controls the IEADs onto the wafer. A similar principle applies to ICPs having a substrate bias. The ICP power is intended to control the magnitude of the ion flux while the bias power is intended to control the IEADs onto the wafer. Since, however, the sheath thickness scales inversely with plasma density, and the properties of IEADs are sensitive to sheath thickness, the goal of totally independent control of ion flux and IEADs is difficult to achieve. This coupling of plasma source power and sheath

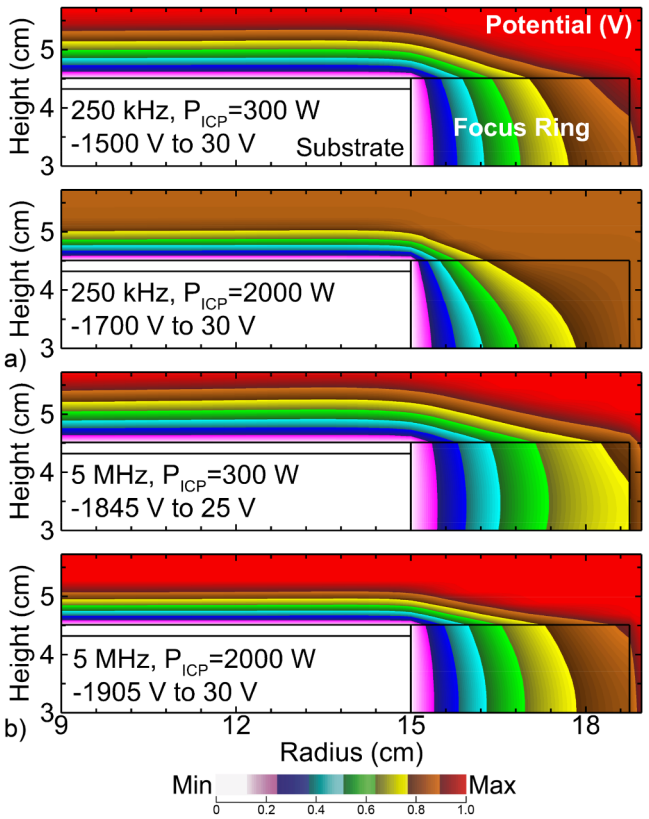

FIG. 13. Electric potential at the peak cathodic part of the RF cycle for bias frequencies of (a) 250 kHz and (b) 5 MHz for 300 W and 2 kW ICP power. The ranges of potential in each image are noted.

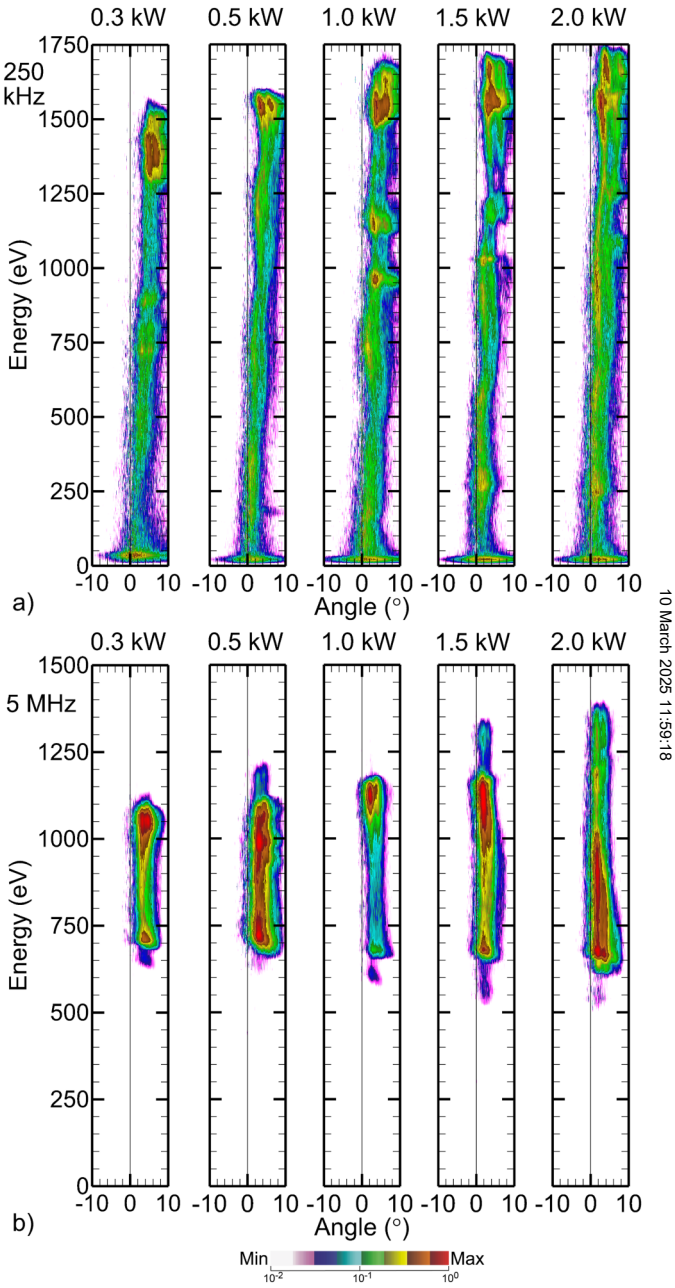

FIG. 14. Ion energy and angular distributions (IEADs) at the edge of the wafer for ICP powers of 300 W to 2 kW for bias frequencies of (a) 250 kHz and (b) 5 MHz. The images are plotted on a two-decade log scale.

properties extends to the curvature of the sheath that affects tilt of the IEADs at the wafer edge.

Electric potentials in the vicinity of the edge of the wafer at the peak of the cathodic portion of the cycle are shown in Fig. 13 for ICP powers of 300 and 2000 W, for bias frequencies of 250 kHz and 5 MHz. With a bias frequency of 250 kHz, the sheath thickness decreases from 0.99 cm with an ICP power of 300 W to 0.57 cm at 2000 W. With a bias frequency of 5 MHz, the sheath thickness decreases from 1.1 cm with an ICP power of 300 W to 0.57 cm at 2000 W. For a constant bias voltage and FR permittivity, the current required to charge the capacitance of the FR is the same. The higher plasma density and ion flux at the higher ICP power enables the FR to be fully charged at either frequency. This more complete FR charging would, absent other effects, lead to more curvature of the sheath.

IEADs at the edge of the wafer for ICP powers of 300 W to 2 KW and bias frequencies of 250 kHz and 5 MHz are shown in Fig. 14. The angular asymmetry (tilt) and width for these powers

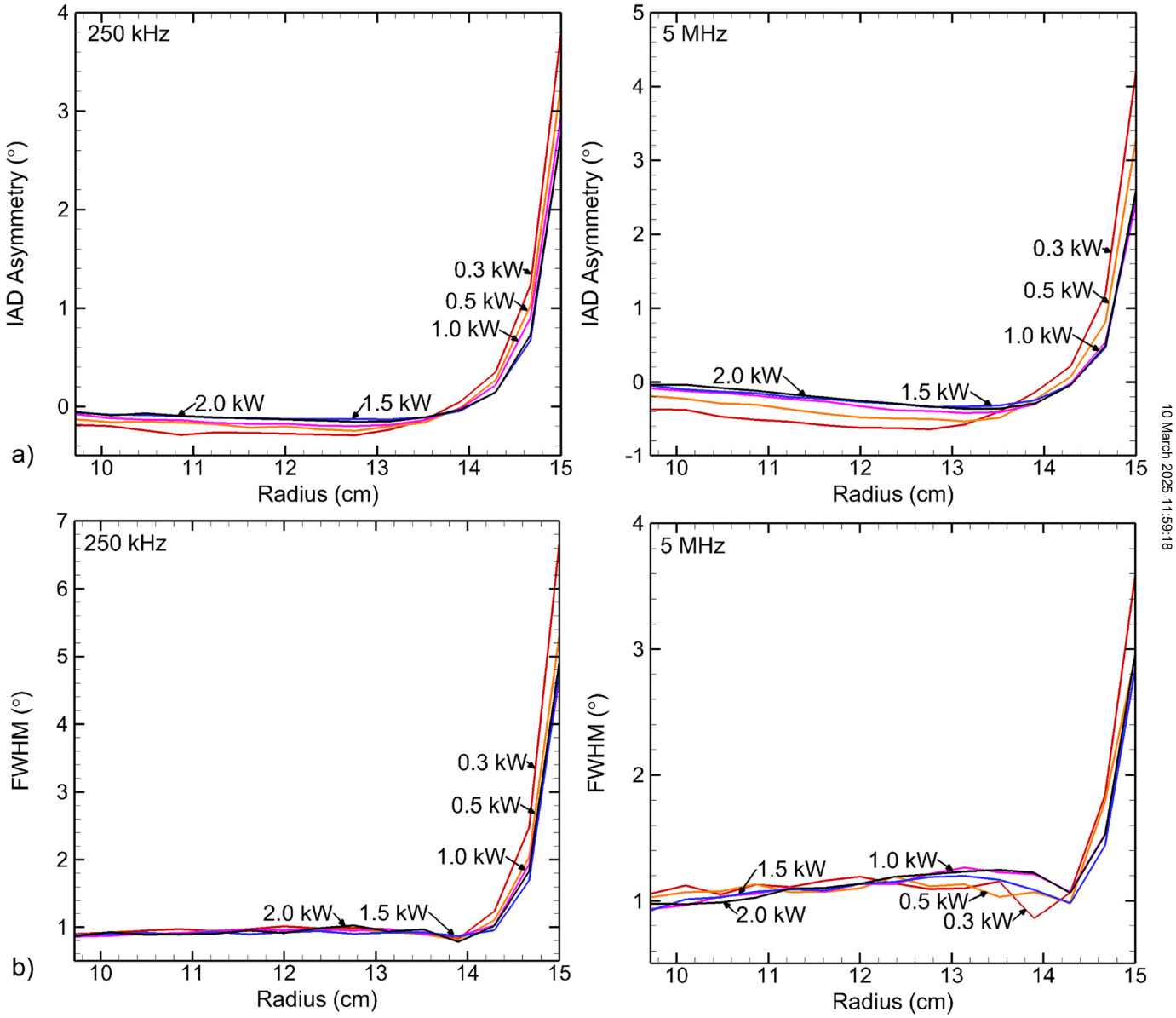

FIG. 15. Angular properties of the IEADs as a function of radius for ICP powers of 300 W to 2 kW. (a) IAD asymmetry (tilt) for bias frequencies of 250 kHz and 5 MHz and (b) FWHM for 250 kHz and 5 MHz.

and frequencies as a function of position on the wafer are shown in Fig. 15. At 250 kHz, V_{DC} spans from −515 V for an ICP power of 300 W to −735 V at 2000 W. At 5 MHz, V_{DC} spans from −835 V for an ICP power of 300 W to −910 V at 2000 W. At both frequencies, the maximum energy of the IEAD increases with increasing power, an effect that is attributable to the thinning of the sheath. For a bias frequency of 250 kHz, the plasma density at the edge of the sheath increased from 1.9×10^9 cm^{-3} to 5.1×10^9 cm^{-3} for ICP powers of 0.3 to 2 kW. At 5 MHz, the plasma density at the edge of the sheath increases from 2.1×10^9 to 3.1×10^9 cm^{-3}. The asymmetries and widths of the IEADs are only weakly dependent on ICP power. For these particular conditions, there are two compensating trends. The thinning of the sheath above the wafer with increasing ICP power should reduce sheath curvature, which would reduce the amount of tilt in the IEAD at the wafer edge. The increase in ion current onto the FR which would more rapidly charge the FR should increase sheath curvature, which would increase the amount of tilt in the IEAD at the wafer edge. The end result is that these

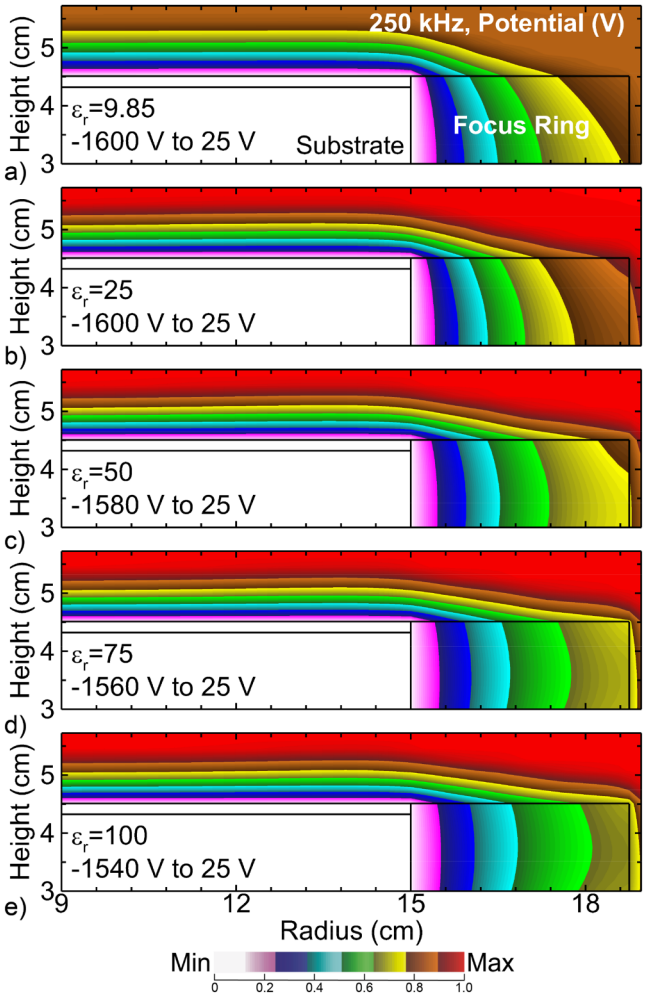

FIG. 16. Electric potential at the peak cathodic part of the RF cycle for a bias frequency of 250 kHz with focus ring relative permittivities ($\varepsilon_r = \varepsilon/\varepsilon_0$) of (a) 9.85, (b) 25, (c) 50, (d) 75, and (e) 100. The ranges of potential plotted in each image are noted.

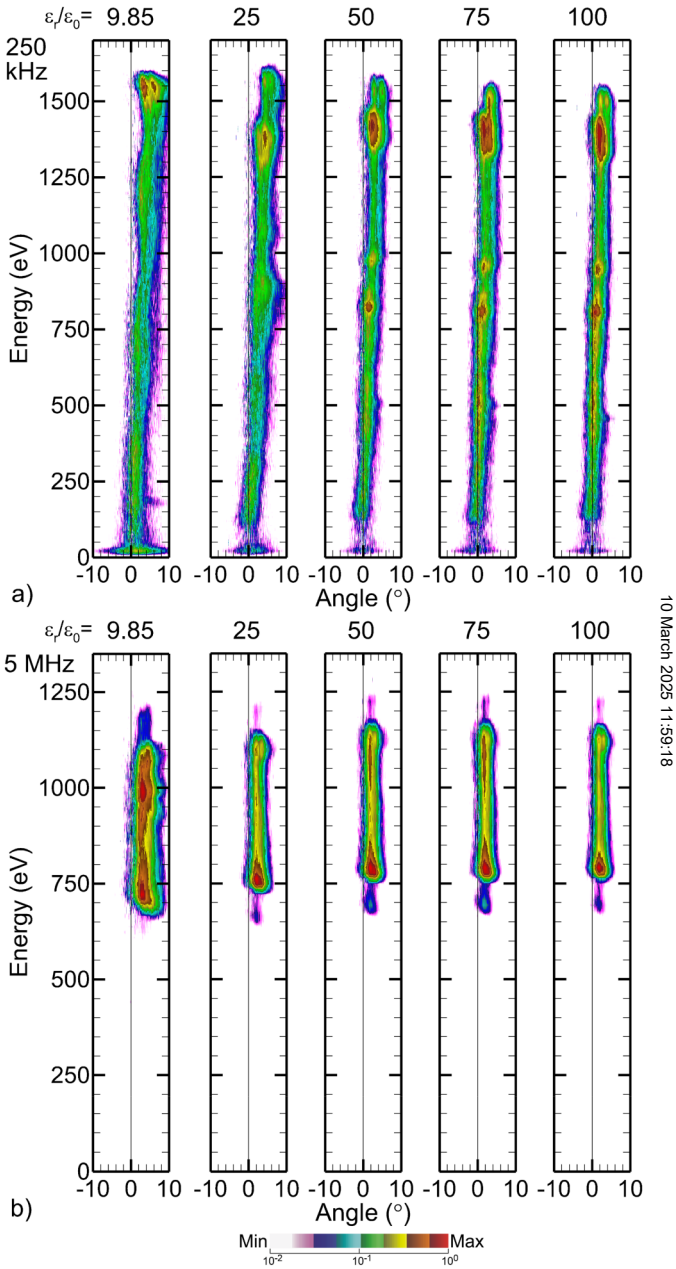

FIG. 17. Ion energy and angular distributions (IEADs) at the edge of the wafer for relative permittivity ($\varepsilon_r = \varepsilon/\varepsilon_0$) of the focus ring of 9.85–100 for bias frequencies of (a) 250 kHz and (b) 5 MHz. The images are plotted on a two-decade log scale.

opposing trends compensate each other, with the ion tilt being not hugely sensitive to ICP power. That said, the tilt is somewhat more severe at the lower powers, a consequence of the large sheath curvature with thicker sheaths over the wafer.

The tilt of the IEADs is more sensitive to ICP power at smaller radii on the wafer than at the edge of the wafer. This sensitivity results from the plasma density becoming less uniform at the higher ICP powers, producing a radially dependent plasma density at the sheath edge. This trend results in a sheath thickness that is a function of radius, which then translates into sheath curvature. In this case, the tilt transitions from being inwards at large radii to outwards at smaller radii. The spread in tilt is less than a degree at radii away from the edge of the wafer. This change in direction of the tilt is highly case dependent. It is also another example of how small changes in operating conditions that produce systematic non-uniformity of plasma density at the edge of the sheath can lead to wafer wide variation in tilt of the IEAD.

The curvature of the sheath at the edge of the wafer is due, in part, to the charging of the focus ring. Charging of the FR reduces the voltage drop and so thickness of the sheath above the FR. The disparity in sheath thickness above the FR and above the wafer than produces curvature in the sheath. Charging of the FR is more problematic at low frequencies as the RF period is longer compared to the RC time constant for charging the FR, and so the FR is charged more fully. Increasing the RC time constant for charging the FR should reduce the charging induced curvature in the sheath and so reduce tilt in the IEAD. This can be accomplished by increasing the permittivity of the FR.

Electric potentials in the vicinity of the edge of the wafer at the peak of the cathodic cycle are shown in Fig. 16 for a bias frequency of 250 kHz and relative permittivity ($\varepsilon_r = \varepsilon/\varepsilon_0$) of the focus ring from 9.85 to 100. With increase in permittivity, the capacitance of the FR increases and, for otherwise the same conditions, the RC time constant for charging the FR increases. With there being less charging of the FR, there is larger potential dissipated in the sheath and the sheath extends further across the FR with less curvature. This concept would, in principle, also apply to a top layer on the FR made of higher permittivity material provided that the series capacitance (top layer and underlying FR) is significantly increased. Since the underlying FR would have the smaller permittivity and be thicker, its smaller capacitance would dominate. One would need a FR structure in which displacement current to the electrode is channeled dominantly through the higher permittivity top layer.

The IEADs' incident onto the edge of the wafer is shown in Fig. 17 for bias frequencies of 250 kHz and 5 MHz for relative permittivity ε_r of the FR from 9.85 to 100. The angular asymmetry of the IEAD as a function of radius for a bias frequency of 250 kHz is shown in Fig. 18 for the same range of permittivity. For a bias

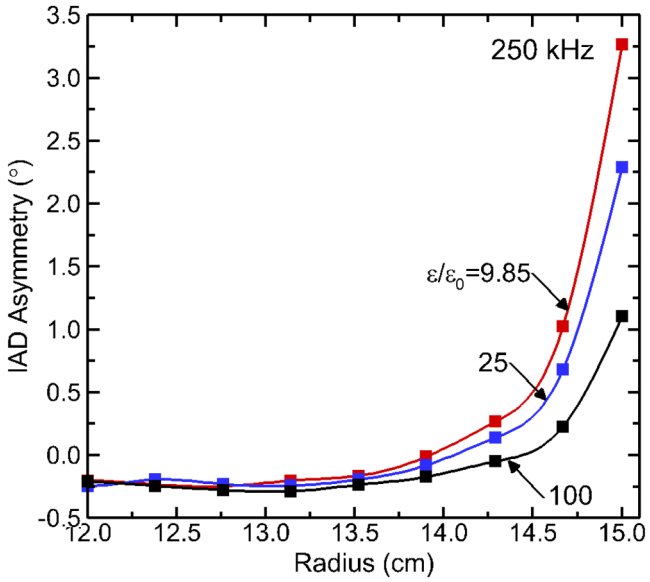

FIG. 18. Asymmetry (tilt) of the IEAD for a bias frequency of 250 kHz as a function of position on the wafer for relative permittivity($\varepsilon_r = \varepsilon/\varepsilon_0$) of the focus ring of 9.85, 25, and 100.

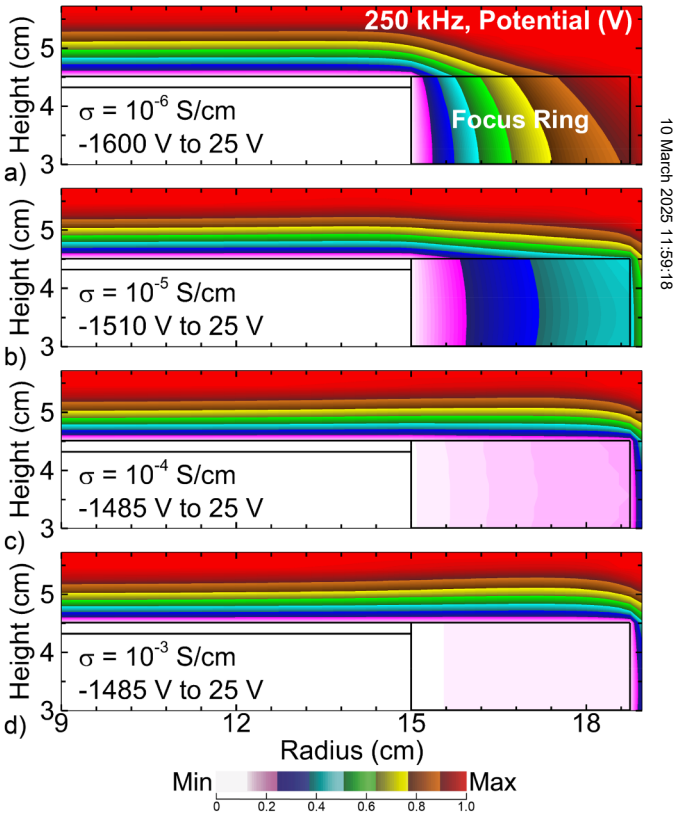

FIG. 19. Electric potential at the peak of the cathodic cycle for a bias frequency of 250 kHz for conductivity of the focus ring of (a) 10^{-6} (b) 10^{-5}, (c) 10^{-4}, and (d) 10^{-3} S/cm. The range of voltage in each image is noted.

frequency of 250 kHz, the decrease in FR charging and decrease in curvature of the sheath with increasing ε_r directly translates into a decrease in tilt of the IEAD. This improvement in the tilt of the IEAD occurs over the entire range of energy, being most impactful at the higher energy where the tilt is usually most severe. The increase in ε_r (and reducing in charging of the FR) enables an increase in displacement current through the FR which is collected by the substrate. This change in current then makes the system look more asymmetric and increases the magnitude of the DC bias. For a bias frequency of 250 kHz, the magnitude of the V_{DC} increases from −610 to −750 V for an increase in ε_r of 9.85–100.

There is only a nominal improvement in tilt of the IEAD with increasing ε_r for a bias frequency of 5 MHz. At the higher frequency, the RF period was already shorter than the RC charging time of the FR with $\varepsilon_r = 9.85$ and so even at the lower permittivity, there was little tilt. Increasing ε_r then had little to improve upon.

Higher permittivity of the FR produced less tilt in the IEADs due to a reduction in FR charging but also because of the intrinsic electrical properties of high dielectric materials. At the boundary between two dielectric materials, the electric field is smaller in the material having the larger permittivity. Based only on polarization of the dielectric, there should be less sheath curvature with a FR having larger permittivity as there would be more voltage allocated to the sheath relative to the material. Another strategy to decrease the electric field (smaller voltage drop) in the FR relative to the sheath is to increase the conductivity of the FR. Assuming that the FR is in physical contact with the powered substrate, this strategy has the added advantage of extending the applied voltage applied to the substrate into the FR. Doing so is the equivalent of extending the radius of the electrode to being greater than that of the wafer which has the effect of maintaining the uniformity of the sheath.

Electric potentials at the peak of the cathodic cycle in vicinity of the wafer edge are shown in Fig. 19 for FR conductivities of $\sigma = 10^{-6}$ to 10^{-3} S/cm and bias frequency of 250 kHz. Increasing the conductivity of the FR serves at least two purposes. The first is to extend the bias voltage beyond the edge of the wafer and to apportion more voltage to the sheath. The second is to conduct away surface charging of the FR which would otherwise remove voltage from the sheath. The end result is that with increasing conductivity of the FR, there is less voltage drop across the FR and less curvature of the sheath. For large values of conductivity, $\sigma > 10^{-4}$ S/cm, the curvature of the sheath reverses. With the potential of the FR nearing that of the electrode while the plasma density above the focus ring is less than that over the wafer, the sheath thickens above the FR. Surface charge dissipation could also be accomplished with a conductive coating on the surface of the dielectric FR. However, the conductive coating would still need to have a path for current to pass through the coating to the powered electrode. Without such a connection, the dielectric FR would still block conduction current. For example, if a wafer-FR gap were to prevent conduction current from the layer from reaching the powered electrode, the conductive layer would simply charge coincidently with the underlying FR.

The IEADs incident on the edge of the wafer for bias frequencies of 250 kHz and 5 MHz are shown in Fig. 20 for conductivities of the FR from $\sigma = 10^{-6}$ to 10^{-3} S/cm. The angular tilt and width of the IEADs as a function of radius are shown in Fig. 21 for FR conductivities of $\sigma = 10^{-6}$ to 1 S/cm. For both frequencies, increasing conductivity of the FR reduces the angular asymmetry and reduces angular width of the IEAD while also reducing the maximum energy. The reduction in maximum energy is attributed to a decrease in the magnitude of the DC bias with increasing conductivity. The magnitude of V_{DC} decreases from −600 to −530 V for a bias

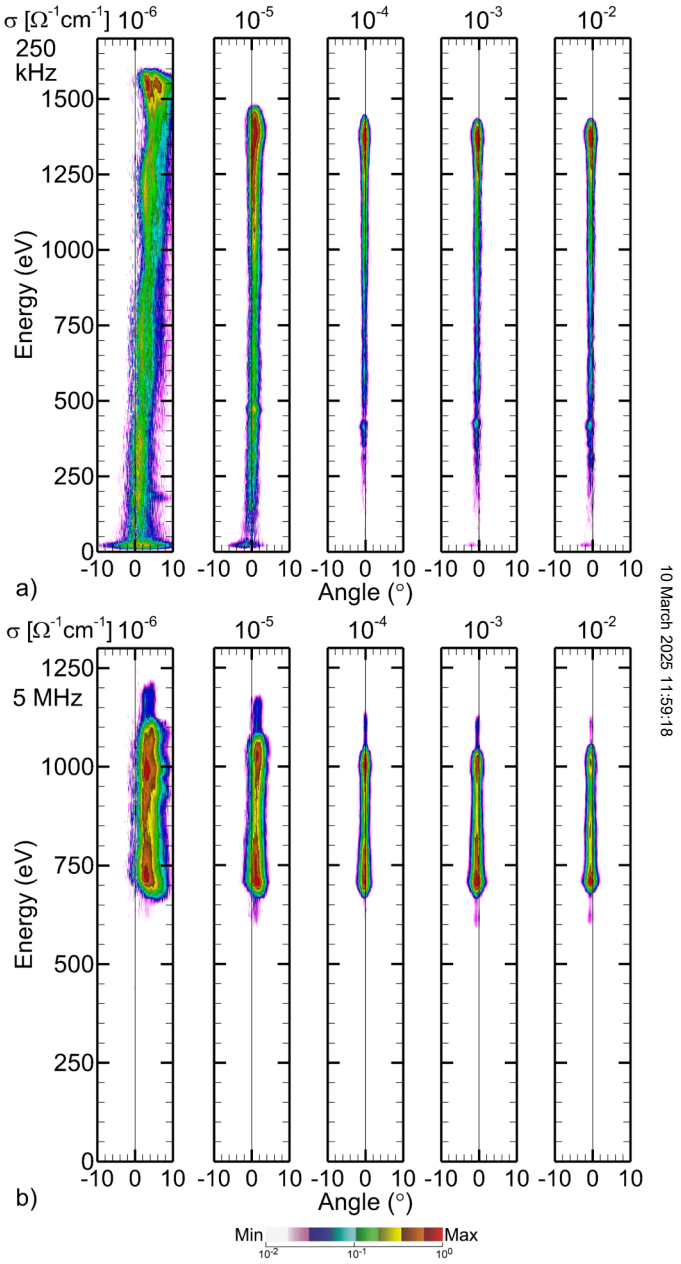

FIG. 20. Ion energy and angular distributions (IEADs) at the edge of the wafer for conductivity of the focus ring of 10^{-6}–10^{-2} S/cm for bias frequencies of (a) 250 kHz and (b) 5 MHz. The images are plotted on a two-decade log scale.

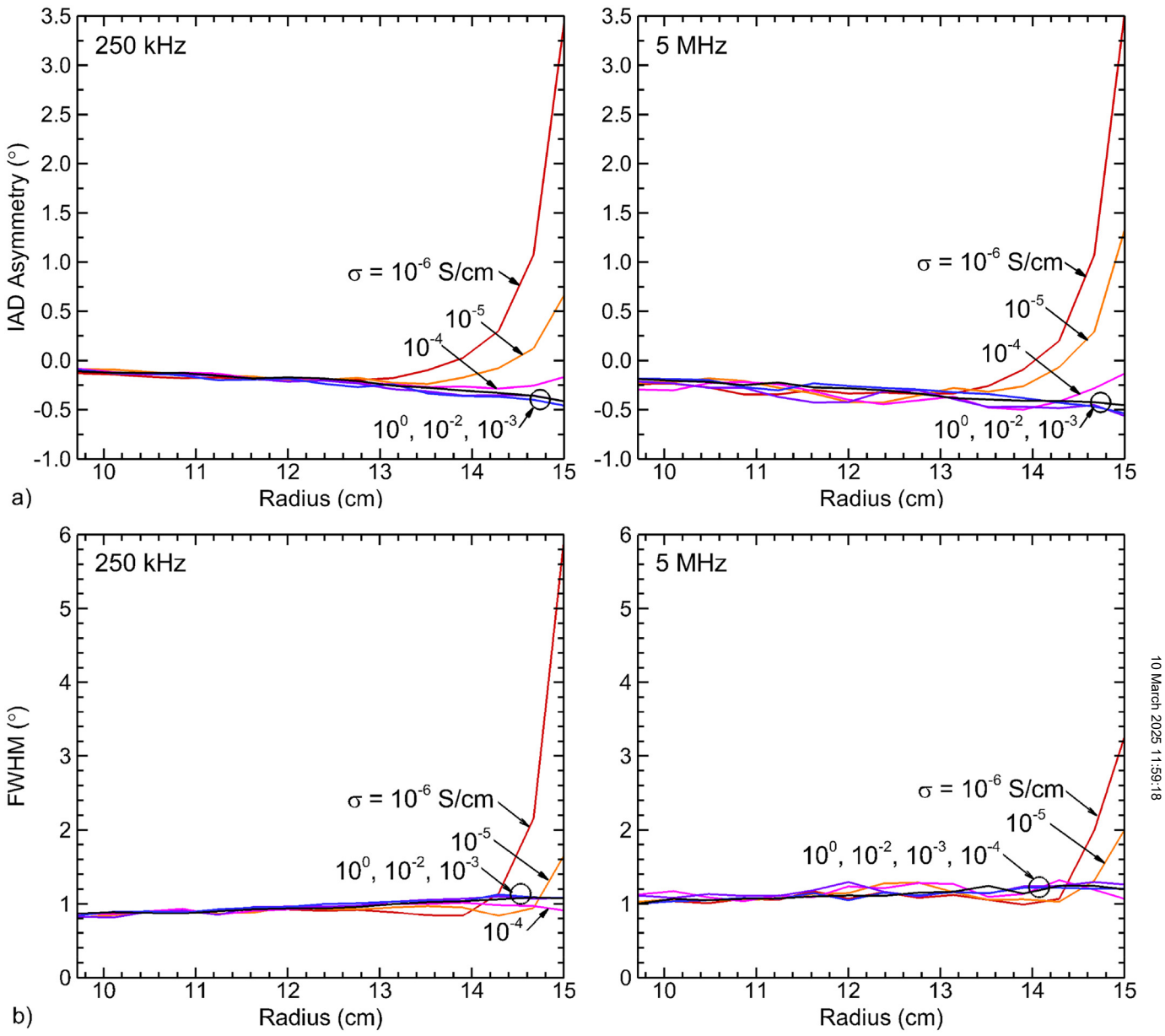

FIG. 21. Angular properties of the IEADs as a function of radius for focus ring conductivities of 10^{-6}–1 S/cm. (a) IAD asymmetry (tilt) for bias frequencies of 250 kHz and 5 MHz and (b) FWHM for 250 kHz and 5 MHz.

frequency of 250 kHz for a FR conductivity of $\sigma = 10^{-6}$ to 10^{-2} S/cm. The higher conductivity FR conveys current to the substrate, making the powered side of the circuit appear to have a larger area. With the there being little voltage dropped across the FR, the sheath potential remains large over the majority of the RF cycle, thereby reducing the low energy component of the IEAD. For both 250 kHz and 5 MHz bias, an angularly symmetric IEAD is achieved with FR conductivities of 10^{-3}–10^{-4} S/cm.

For these particular conditions, there is a small outward tilt to the IEAD across the wafer. This small tilt is highly condition dependent and largely independent of the wafer-edge tilting due to FR properties. The outward tilt of the IEAD (<0.5°) results from the ionization source and plasma density that are off axis (see Figs. 2 and 3). These conditions produce a shallow tilt to the sheath edge across the wafer. With the increase in conductivity of the FR, the inward tilt of the IEAD at the edge of the wafer is

largely eliminated and reverses to be outwardly tilted to align with the sheath across the remainder of the wafer. The angular width of the IEAD decreases with increasing FR conductivity, following a similar trend as the tilt. The minimum angular width of the IEAD is achieved with FR conductivities of 10^{-5} to 10^{-4} S/cm.

V. CONCLUDING REMARKS

A computational investigation was performed on the origins and causes of angular tilt of the IEAD near the wafer edge in ICPs having low frequency (<1 MHz) substrate biases. The plasma was sustained in an $Ar/Cl_2/O_2$ mixture at 15 mTorr, with bias frequencies of 250 kHz to 5 MHz, bias amplitudes of 500–5000 V and ICP power of 300–2000 W, while varying the permittivity and conductivity of the FR. A summary of key findings follow, with more extended discussion:

- Low substrate bias frequencies have RF periods greater than ion sheath traversal time, increasing maximum ion energies and narrowing angular spread of ions incident onto the wafer.
- Low bias frequencies increase the impedance of the dielectric FR, reducing the sheath voltage and sheath thickness as a function of radius across the FR.
- With decreasing frequency, the RF period becomes commensurate with the RC time constant for charging of the FR, leading to greater FR charging and increasing curvature of the sheath at the wafer-FR interface. The additional sheath curvature results in more ion angular skew at the edge of the wafer.
- Higher bias voltages produce thicker sheaths that have increased sheath curvature, particularly at lower frequencies, increasing ion tilt at the wafer edge.
- Increasing ICP power leads to increased plasma density which reduces sheath thickness and reduces sheath curvature at the edge of the wafer.
- Increasing FR permittivity increases FR capacitance and decreases FR impedance which reduces voltage drop in the FR while retaining voltage drop in the sheath over the FR. There is less sheath curvature and less ion tilt.
- A higher conductivity FR produces a more uniform sheath across the edge of the wafer FR, reducing sheath curvature and ion tilt.

Across the majority of the wafer, decreasing the bias frequency achieved the desired goals of extending the IEAD to higher energies while narrowing the angular distribution. These desirable characteristics were not fully retained to the edge of the wafer. With the low conductivity FR acting as a capacitor, charging of the FR removes voltage from the bounding sheath leading to curvature of the sheath at the edge of the wafer. This curvature then produces an angular tilt and increase in angular breadth to the IEAD at the edge of the wafer. Low frequencies with larger RF periods relative to the RC time constant for charging the FR produce more curvature of the sheath and larger tilt in the IEAD. Tilt of the IEAD at low frequencies is most severe at the highest ion energies. The sheath curvature is most severe for thick sheaths which occur at the maximum of the cathodic portion of the cycle. In the thin-sheath limit that occurs at the lowest frequencies, ions cross the sheath in a small fraction of the RF period, and so the high energy ions are imprinted with the angular skew of the sheath at the peak of the cathodic cycle. These effects are somewhat moderated by an increase in the magnitude (more negative) of the DC bias with increasing frequency, resulting in less curvature of the sheath than would have otherwise been produced at lower frequencies.

These trends also apply to the higher frequencies, however, to a lesser extent. Tilting of and angular broadening of the IEAD at the edge of the wafer are less severe than at low frequencies. At frequencies of several MHz to 5 MHz, ion transport is in the thick sheath limit, and so ions average the curvature of the sheath from its most severe at the peak of the cathodic cycle to the least severe curvature at the peak of the anodic cycle. The benefit is that the highly skewed IEAD at high energies produced with frequencies of several hundred kHz does not occur at the higher frequencies. Independent of averaging sheath properties, the shorter RF period at the higher bias frequencies result in less charging of the FR, leaving more voltage to be dissipated across the sheath above the FR. This sheath voltage is more commensurate with that over the wafer, producing less sheath curvature and less tilt to the IEAD at the edge of the wafer.

Those trends extended to varying bias voltage and ICP power. Increasing bias voltage produces thicker sheaths which at the peak of the cathodic cycle produce more sheath curvature at the edge of the wafer, in turn producing a larger tilt to the IEAD. Again, the effect was more severe at lower bias frequencies. Increasing ICP power produced higher plasma densities and thinner sheaths over the wafer, which would, absent other effects, reduce sheath curvature at the edge of the wafer and produced less tilt to the IEADs. However, higher ICP power also increased the rate of FR charging which should produce more tilt to the IEADs. For our conditions, the reduction in sheath thickness dominated with increasing ICP power, resulting in reducing the skew of the IEAD at the edge of the wafer.

The electrical properties of the FR were also influential in controlling the angular tilt and angular breadth of the IEADs at the edge of the wafer. By increasing the permittivity of the FR, the RC time constant required to fully charge the FR increased. For a given RF period, reducing the charging of the FR reduces sheath curvature. For long RF periods at low frequencies, the reduction in sheath curvature reduced the angular tilt of the IEAD at the edge of the wafer. Apart from the benefits of operating with FR having higher dielectric constants, higher FR conductivity was particularly effective in reducing angular tilt and angular breadth of the IEADs at the edge of the wafer. This benefit came from reducing the charging of the FR by conducting away surface charge and from extending the bias voltage beyond the edge of the wafer. For our conditions, a FR conductivity of 10^{-4} S/cm provided near normal IEADs at the edge of the wafer, with larger conductivities producing an outward tilt.

For our conditions, the IEADs incident onto the 30 cm diameter wafer at radii <14 to 14.5 cm generally had tilts of less than 0.5° directed outward. The tilt produced by sheath curvature at the edge of the wafer points inward. While varying, for example, ICP power and bias voltage, local maxima were produced in the tilt of the IEAD over the wafer. In some cases, the tilt reversed directions from outward to inward. These tilts, and their variation, are small (a few tenths of a degree) and result from a combination of small slopes in the sheath over the wafer, and non-normal ion trajectories as the ions enter the sheath. In the absence of a shallow slope in the over-wafer sheath, the angle of an ion

striking the wafer after passing through a collisionless sheath is $\theta = \tan^{-1}(v_{\parallel}/v_{\perp}) \approx \tan^{-1}[(k_B T_I/qV_S)^{1/2}]$, where $v_{\parallel}$ is the velocity parallel to the sheath when the ion enters the sheath, $v_{\perp}$ is the perpendicular velocity at the wafer, T_I is the effective ion temperature at the sheath edge, and V_S is the sheath potential. For an ion approaching the sheath with a parallel velocity corresponding to 0.1 eV with a sheath potential of 1000 V, the corresponding angle at the wafer is about 0.6°. Small deviations from the normal of the velocity of an ion accelerated through a presheath will produce these small tilts over the wafer.

A key takeaway is that varying bias frequency in process design of plasma etching reactors is not independent from the choice of plasma facing materials and their permittivity and conductivity. Future work could address more a deliberate matching of the impedances of these plasma facing materials with the dynamics of the system on both the RF period (frequency) and the pulsing period.

ACKNOWLEDGMENTS

This work was supported by Samsung Electronics Co. The authors thank Scott Doyle (University of Aberdeen) for discussions on the topic of this paper.

AUTHOR DECLARATIONS

Conflict of Interest

The authors have no conflicts to disclose.

Author Contributions

Evan Litch: Conceptualization (equal); Formal analysis (lead); Investigation (lead); Methodology (lead); Software (equal); Validation (lead); Visualization (lead); Writing – original draft (lead); Writing – review & editing (equal). **Hyunjae Lee:** Conceptualization (equal); Project administration (equal); Resources (equal); Supervision (equal); Writing – review & editing (equal). **Sang Ki Nam:** Conceptualization (equal); Project administration (equal); Resources (equal); Supervision (equal); Writing – review & editing (equal). **Mark J. Kushner:** Conceptualization (equal); Formal analysis (equal); Funding acquisition (equal); Project administration (equal); Resources (equal); Software (equal); Supervision (equal); Writing – review & editing (equal).

DATA AVAILABILITY

The data that support the findings of this study are available from the corresponding authors upon reasonable request.

REFERENCES

[1]I. Adamovich *et al.*, J. Phys. D: Appl. Phys. **55**, 373001 (2022).
[2]G. S. Oehrlein and S. Hamaguchi, Plasma Sources Sci. Technol. **27**, 023001 (2018).
[3]K. Ishikawa, K. Karahashi, T. Ishijima, S. Il Cho, S. Elliott, D. Hausmann, D. Mocuta, A. Wilson, and K. Kinoshita, Jpn. J. Appl. Phys. **57**, 06JA01 (2018).
[4]H. Tanaka *et al.*, "Bit cost scalable technology with punch and plug process for ultra high density flash memory," in *2007 IEEE Symposium on VLSI Technology, Kyoto, Japan* (IEEE, New York, 2007), pp. 14–15.
[5]S.-N. Hsiao, K. Ishikawa, T. Hayashi, J. Ni, T. Tsutsumi, M. Sekine, and M. Hori, Appl. Surf. Sci. **541**, 148439 (2021).
[6]H. W. Tak *et al.*, Appl. Surf. Sci. **600**, 154050 (2022).
[7]C.-F. Han, C.-C. Lin, and J.-F. Lin, Precision Eng. **71**, 141 (2021).
[8]E. G. Shustin, J. Commun. Technol. Electron. **62**, 454 (2017).
[9]B. R. Rogers and T. S. Cale, Vacuum **65**, 267 (2002).
[10]G.-R. Lee, S.-W. Hwang, J.-H. Min, and S. H. Moon, J. Vac. Sci. Technol. A **20**, 1808 (2002).
[11]J.-H. Min, G.-R. Lee, J. Lee, S. H. Moon, and C.-K. Kim, J. Vac. Sci. Technol. B **22**, 893 (2004).
[12]E. Kawamura, V. Vahedi, M. A. Lieberman, and C. K. Birdsall, Plasma Sources Sci. Technol. **8**, R45 (1999).
[13]Y. Zhang, J. Liu, Y. Liu, and X. Wang, Phys. Plasmas **11**, 3840 (2004).
[14]M. A. Sobolewski, J. K. Olthoff, and Y. Wang, J. Appl. Phys. **85**, 3966 (1999).
[15]T. Tran *et al.*, in *2004 IEEE/SEMI Advanced Semiconductor Manufacturing Conference and Workshop (IEEE Cat. No.04CH37530)* (IEEE, New York, 2004) pp. 453–460.
[16]M. Y. Yoon, H. J. Yeom, J. H. Kim, J.-R. Jeong, and H.-C. Lee, Appl. Surf. Sci. **595**, 153462 (2022).
[17]I. Seong, J. Lee, S. Kim, Y. Lee, C. Cho, J. Lee, W. Jeong, Y. You, and S. You, Nanomaterials **12**, 3963 (2022).
[18]H. Džafić, M. R. Kamali, and S. P. Venugopalan, J. Phys. D: Appl. Phys. **55**, 075201 (2022).
[19]F.-F. Ma, Q.-Z. Zhang, D.-M. Han, Z.-L. Xiong, M. Gao, and Y.-N. Wang, J. Vac. Sci. Technol. A **41**, 053002 (2023).
[20]J. S. Kim, M. Y. Hur, H. J. Kim, and H. J. Lee, J. Appl. Phys. **126**, 233301 (2019).
[21]H. C. Kim and V. I. Manousiouthakis, J. Vac. Sci. Technol. B **18**, 841 (2000).
[22]N. Schmidt, J. Schulze, E. Schüngel, and U. Czarnetzki, J. Phys. D: Appl. Phys. **46**, 505202 (2013).
[23]Y.-R. Zhang, Y.-T. Hu, and Y.-N. Wang, Plasma Sources Sci. Technol. **29**, 084003 (2020).
[24]M. J. Kushner, J. Phys. D: Appl. Phys. **42**, 194013 (2009).
[25]F. Krüger, H. Lee, S. K. Nam, and M. J. Kushner, J. Vac. Sci. Technol. A **41**, 013006 (2023).
[26]P. Tian and M. J. Kushner, Plasma Sources Sci. Technol. **26**, 024005 (2017).
[27]S. Huang, V. Volynets, J. R. Hamilton, S. Lee, I.-C. Song, S. Lu, J. Tennyson, and M. J. Kushner, J. Vac. Sci. Technol. A **35**, 031302 (2017).
[28]S. Tinck, W. Boullart, and A. Bogaerts, Plasma Sources Sci. Technol. **20**, 045012 (2011).
[29]P. Zhang, L. Zhang, and K. Lv, Plasma Chem. Plasma Process. **40**, 1605 (2020).
[30]G. S. Hwang and K. P. Giapis, J. Appl. Phys. **82**, 566 (1997).
[31]J.-H. Kim, Y.-H. Shin, and K.-H. Chung, Thin Solid Films **435**, 288 (2003).
[32]B. G. Heil, U. Czarnetzki, R. P. Brinkmann, and T. Mussenbrock, J. Phys. D: Appl. Phys. **41**, 165202 (2008).
[33]B. P. Wood, M. A. Lieberman, and A. J. Lichtenberg, IEEE Trans. Plasma Sci. **23**, 89 (1995).
[34]M. A. Lieberman, A. J. Lichtenberg, E. Kawamura, T. Mussenbrock, and R. P. Brinkmann, Phys. Plasmas **15**, 063505 (2008).
[35]T. Lafleur and P. Chabert, Plasma Sources Sci. Technol. **24**, 044002 (2015).
[36]M. A. Lieberman and A. J. Lichtenberg, *Principles of Plasma Discharges and Materials Processing* (Wiley, New York, 2005).
[37]E. C. Benck, A. Schwabedissen, A. Gates, and J. R. Roberts, J. Vac. Sci. Technol. A **16**, 306 (1998).
[38]L. Huang and Q. Wang, J. Phys. Conf. Ser. **2433**, 012002 (2023).